No.2022–04–05

Virtual Suspension Control for a Two-Wheeled Mobile Transport Robot

Virtual Suspension Control in Two-Wheeled Transport Robot

Supervisor: Professor Toshiyuki Murakami

Keio University, Faculty of Science and

Technology, Department of System Design Engineering

Graduation Thesis for 2022 (Reiwa 4)

Student ID number: 61919602

Makoto Onnazawa

table of contents

Table of Contents

Table Contents

Chapter 1

Introduction

1.1 Research Background

1.1.1 Current state of logistics

Due to the impact of COVID-19, the BtoC-EC market size has increased significantly since 2020 [1]. Figure 1-1 shows the trends in the BtoC-EC market size and EC conversion rate in the product sales sector over time.

The average annual growth rate of the BtoC-EC market size in the product sales sector from 2019 to 2021 is expected to be approximately 15%.

Many retailers have begun to check the actual products in their physical stores due to the spread of COVID-19.

Fig. 1-1: Changes in the BtoC-EC market size and EC conversion rate over time in the product sales sector [1]

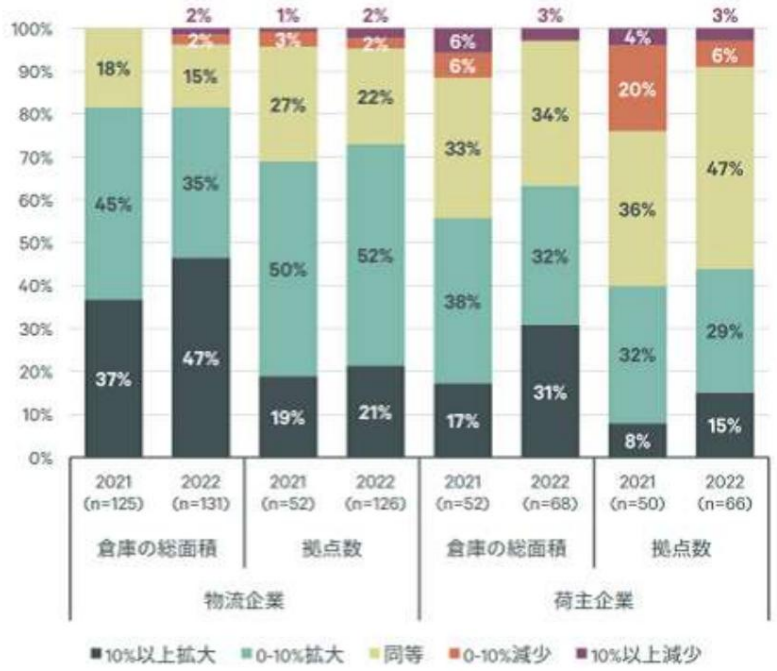

Fig. 1-2: Warehouse expansion plans of logistics companies and shippers over the next three years [2]

They have also started initiatives such as showrooming stores to encourage online purchases and online customer service . Therefore, the BtoC-EC market is expected to continue to grow in size.

In addition, according to a CBRE survey of logistics facility tenants [2] , more than 80% of logistics companies More than 60 % of shippers responded that they plan to expand their warehouse space over the next three years. Fig. 1-2 shows the warehouse expansion plans of logistics companies and shippers over the next three years.

As the demand for logistics increases, the demand for transport robots in warehouses is also expected to increase. According to Yano Research Institute [3] , the number of shipments of automated guided vehicles (AGVs) and autonomous mobile robots (AMRs) is The shipment volume is predicted to grow to 9,950 units in fiscal year 2025. Fig. 1-3 shows the trends and forecasts of the shipment volume of AGV/AMR (transport robots).

1.1.2 Transport robots used in logistics

In the logistics field, there are various transport robots, especially forklifts, AGVs, and AMRs. Fig. 1-4 shows an example of an unmanned forklift from Toyota Land Fleet [4] , and Fig. 1-5 shows an example of an AGV from Mujin Co., Ltd. [5] .

A forklift is a cargo handling and transport machine equipped with a mast that uses power to raise and lower forks.

Fig. 1-3: Trends and forecasts of AGV/AMR (transport robot) shipments [3]

Fig. 1-4: Unmanned forklift [4]

Fig. 1-5: AGV[5]

In the field of logistics, it is used for unloading and loading cargo from trucks and racks, and for transporting luggage.
Among forklifts, counterbalance forklifts have a stable body.
It is widely used because it can carry heavy objects. A counterbalanced forklift is a forklift that has a counterweight mounted on the rear of the vehicle.

Even when heavy objects are loaded onto the forks at the front of the vehicle, the weight of the objects being transported can be controlled by the
However, it is possible to prevent the vehicle from tipping forward due to the counter-force.
The weight of the weight requires extra energy and reduces energy efficiency.
There are challenges.

AGVs are robots that transport goods by traveling along fixed routes set by magnetic tapes, etc.
AMR uses sensors to grasp the surrounding situation and calculates the
AGVs and AMRs are robots that transport goods by traveling along a route.
Both types of robots have the disadvantage of being weak when moving over uneven surfaces.
If the driving wheels are lifted due to unevenness in the surface, obstacles will occur to the vehicle.
However, if the unevenness of the floor means that all the wheels are not in contact with the ground, problems will occur.
When introducing a new type of machine , it is necessary to make the floor of the warehouse or factory sufficiently flat, which increases costs.
This has the problem of being susceptible to

A robot that can solve the problems faced by forklifts, AGVs , and AMRs.
One example is a two-wheeled mobile robot.

The two-wheeled mobile robot is an inverted pendulum robot that moves in a translational direction using two wheel motors on the left and right.
It is necessary to control three degrees of freedom: the direction, the turning direction, and the pitch angle direction, which is the inclination of the body.
Therefore, the two-wheeled mobile robot has a statically unstable structure, but the posture stabilization
By applying control, it is possible to maintain the inverted state.

The two-wheeled mobile robot can transport objects without using a counterweight by implementing posture stabilization control.
In addition, two-wheeled mobile robots have high rough terrain traversal capabilities, making them ideal for use in warehouses and factories.
No special construction is required for floors.

1.1.3 Challenges associated with operating in a warehouse

Warehouses are environments where condensation is likely to occur . [6] The reason is that warehouses are made of concrete.
and that its structure makes ventilation difficult.

It is known that concrete buildings are prone to condensation [7]. Concrete absorbs water.
Concrete also has high thermal conductivity and moisture retention.

Fig. 1-6: Tire chains [8]

Because the temperature is high, heat and cold are absorbed and are difficult to escape. Therefore, it becomes easy for a temperature difference to occur with the outside air.
This can cause condensation.

Warehouses need to utilize the space, so they tend to be large spaces with high ceilings and few partitions.
In addition, there are few windows in warehouses, and they often cannot be opened, so ventilation is difficult.
The poor air conditioning efficiency and poor ventilation make it difficult to regulate humidity.
This is difficult and can cause condensation.

Furthermore, in a refrigerated warehouse, temperature differences are likely to occur, especially near the entrance and exit of the warehouse.
Dew is likely to form.

When condensation occurs and the floor is wet, the risk of the robot slipping increases.
In order to improve the transportation efficiency of the vehicle, acceleration/deceleration and turning are required frequently.
The higher the height, the higher the risk of slipping.
As shown above, it is difficult to predict the slipperiness of the floor surface and control it accordingly. Therefore, it is necessary to implement measures in the mechanism to prevent slipping.

To deal with slippage, the wheels are made uneven to reduce the contact area with the ground,
It is believed that increasing the grip force is effective. Methods for adding irregularities to the wheel shape include:
One method is to attach chains to the wheels. Fig. 1-6 shows an example of a chain.

However, when the wheels are made uneven, vibrations occur in the vehicle body depending on the shape of the wheels.
This is inconvenient for transport robots because it transmits vibrations to the items being transported.

Therefore, in this study, we focus on the vibration of the transported object in a two-wheeled mobile transport robot.

Fig. 1-7: Segway X2 SE[9]

Fig. 1-8: Winglet [10]

1.2 Position of this paper

A variety of research projects have been conducted on two-wheeled mobile robots.

Because of its high maneuverability and excellent rough terrain traversal performance, it has already been put to practical use in the mobility field, and the Segway

Some of these have been commercialized, such as the Segway X2 SE from the company [9] and the Winglet from Toyota Motor Corporation [10] .

The Segway uses a sensor to read the forward and backward tilt caused by the movement of the person's center of gravity, and responds accordingly .

The robot moves, so it is easy to operate intuitively. Winglet is a rider-type two-wheeled mobile robot, and a public road

running experiment was conducted on the waterfront of Tokyo for one year from March 2016. Segway and Winglet

are shown in Fig. 1-7 and Fig. 1-8 , respectively .

Regarding research on two-wheeled mobile robots, F. Grasser et al. [12] linearized the robot near the equilibrium point, which is the inverted balance state.

In addition, K. Pathak et al . [13] performed a partial linearization field to achieve attitude stabilization.

By performing feedback, we derived a new model and used it to stabilize the posture.

There is also a lot of research being done on two-wheeled mobile robots for people to use as mobility devices.

[14] achieved attitude stabilization by determining the control input based on the Lyapunov stability theorem, and

We have developed a two-wheeled wheelchair that can move forward and backward by shifting the center of gravity.

The pitch angle disturbance observer (PADO) compensates for disturbances in the wheel drive direction.

By introducing a disturbance observer (DOB) [15] , a robust control system against disturbances and modeling errors was

constructed. Kuramatsu [16] used repulsive compliance control (RCC) to measure the disturbances applied by the passenger .

In this study, a pitch angle command value in the opposite direction to the pitch angle command value was generated to compensate for the deviation in the center of gravity position, thereby

suppressing unintended acceleration of the vehicle body. Kim [17] used a joint pitch angle disturbance observer (SPADO) to detect the disturbance applied to the pitch angle and the vehicle

We succeeded in compensating for the disturbances acting on the loop using a single observer.

As a research on the tracking ability of two-wheeled mobile robots, Hatakeyama et al. [18][19] has proposed a method to control the high-speed movement of an inverted pendulum.
One of the studies on control is the zero dynamics obtained by applying partial linearization to the dynamics of an inverted pendulum.
By taking into account the mix of the two wheels and intentionally inputting an angle that makes the attitude angle unstable,
This is a control system design that enables the bot to move at high speed.

There is also research using two-wheeled mobile robots as transport robots .
Sekiguchi [21] analyzed the effect of the height of the center of gravity on the stability of the robot, and
In order to respond to changes in the center of gravity and the steering angle, model-following control was performed on the output speed of the vehicle body.

There has been a lot of research into two-wheeled mobile robots, and the two-wheeled mobile robot is now being used as a transport robot.
However, previous studies have not considered the effects of external disturbances on the payload.
In logistics, it is essential to maintain the quality of the transported goods.
If the product is subjected to vibration or shaking, the exterior may be crushed, scratched, or dented.
If the shaking is large, there is a risk of internal or external damage to the products being transported.
A robot must deal with external disturbances or vibrations and swings caused by the robot itself.
Therefore, in this paper, we propose a method to prevent the fork part on which the transported object is placed from being disturbed by external disturbances or the robot itself.
The control system suppresses the effects of vibrations and swaying on the transported goods by making the goods move in accordance with the vibrations and swaying that occur during transport.
We constructed the following.

1.3 Overview of this paper

The two-wheeled mobile transport robot used in this study is shown in Fig. 1-9 .
The vehicle is fitted with forks driven by a motor, and cargo is transported by loading it onto the forks.

In this paper, we consider the generation of vibrations that occur during transportation on the forks of a two-wheeled mobile transport robot.
The purpose of this study is to suppress the impact of the impact.
The impact force is the mass multiplied by the acceleration, but the mass of the transported object does not change.
The impact of the shock was evaluated based on the magnitude of the acceleration.
To achieve this, we propose implementing compliance control for the fork of the robot. Fig. 1-10 shows a comparison diagram of the case where the proposed method is not used and the case where the proposed method is used. By using compliance control, the movement of the fork is controlled according to the force applied to it.
The input of the torque control is the reaction torque on the fork estimated by the reaction torque observer (RTOB).
However, if the RTOB value is used as input, the gravity of the transported object will be

Fig. 1-9: The two-wheeled mobile transport robot used in this paper

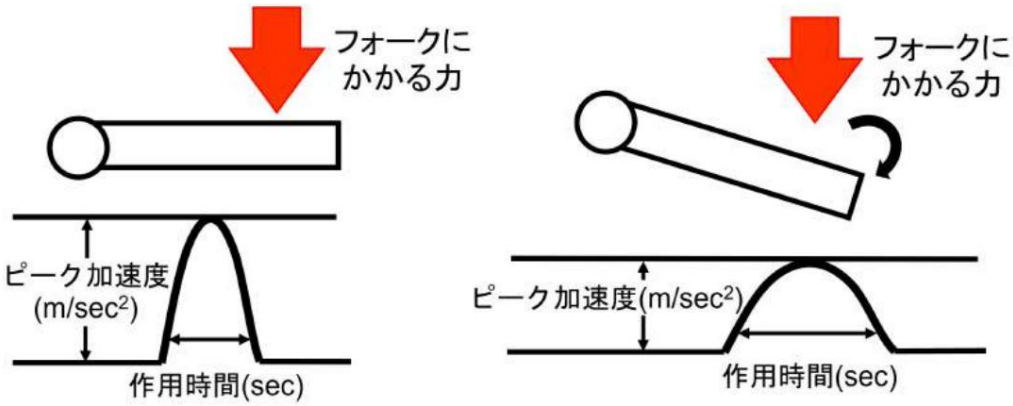

Fig. 1-10: Comparison between conventional and proposed methods

If the forks continue to tilt, they will drop the load and become unusable for transportation.

This was addressed by eliminating the DC component from the

1.4 Structure of this paper

This paper is structured as follows. In Chapter 2 , we model the two-wheeled mobile transport robot that is the subject of this paper. In Chapter 3 , we explain the control system design, including the proposed method. In Chapter 4 , we conduct experiments. The effectiveness of the proposed method is verified by the following. Finally, the conclusion of this paper is given in Section 5 .

Chapter **2**

modeling

In Chapter 2 , we model the two-wheeled mobile transport robot that is the object to be controlled. First, we define the coordinate system and the position and orientation of the robot as kinematics, and consider the constraint conditions. Next, we consider the dynamics. The energy of the two-wheeled mobile transport robot is derived by the Lagrangian method, and then the equation of motion is calculated. After deriving the equation without considering the constraints, we obtain the reduced-dimensional equation of motion including the constraints. Finally, since this study only deals with movement in the straight line, we use a lower dimensional equation for simplicity: The model is shown below.

2.1 Kinematics

2.1.1 Definition of coordinate system and position and orientation of two-wheeled mobile transport robot

In this subsection, we will explain the coordinate system and the two-wheeled transport robot modeling. The position and posture of the robot are defined. Fig. 2-1 shows a top view of the two-wheeled mobile transport robot, and Fig. 2-2 shows the A side view is shown.

The vehicle coordinate system ÿv{Xv, Yv, Zv} is defined at the center of the wheels of the two-wheeled mobile transport robot . ÿv is the world coordinate system . The robot is located at the position of equation (2.1) when viewed from the coordinate system ÿW{XW, YW, ZW} , and ÿ is the rotation angle of the robot when viewed from ÿW , that is, That is, it indicates the angle between the XW axis and the Xv axis. Also, R indicates the wheel radius.

$$P_v^W = [xv, yv, R]^T \tag{2.1}$$

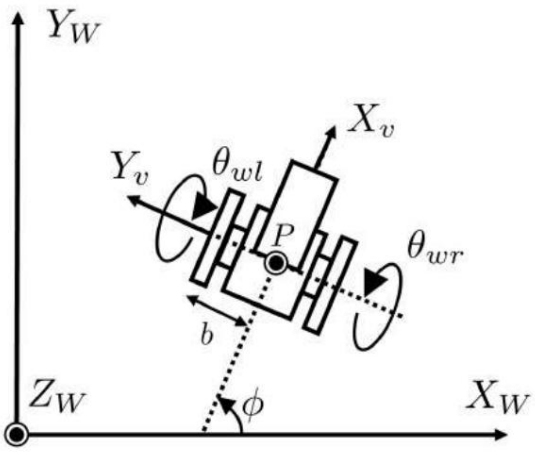

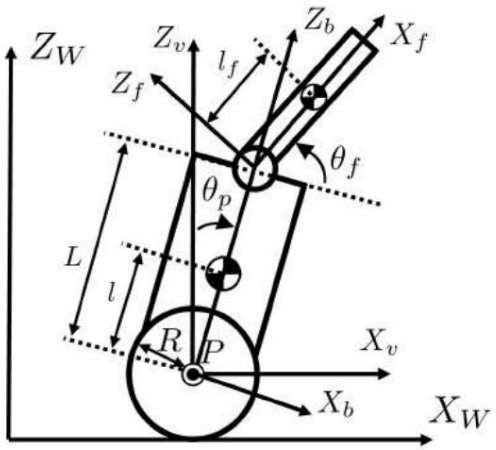

Fig. 2-1: Top view of the two-wheeled mobile transport robot Fig. 2-2: Side view of the two-wheeled mobile transport robot

Define a body coordinate system ÿb{Xb, Yb, Zb} inside the vehicle body . ÿb is a coordinate system inclined by ÿp around the Yv axis of ÿv . The point translated upward in the Zb direction is the center of mass of the body .

Define the fork coordinate system ÿf{Xf , Yf , Zf} at the base of the fork . ÿf as seen from the body coordinate system ÿb is at a point translated upward by L in the Zb direction, and rotates around the Yf axis by ÿf . The point translated upward by lf in the Xf direction is the center of mass of the fork.

Hereafter, we use the simplification of equation (2.2) for the angle difference .

$$ÿf ÿ ÿp = ÿfÿp \tag{2.2}$$

The coordinate of the control reference point P in the world coordinate system is XW , the coordinate of the center of the right wheel is XWwr , and the coordinate of the center of the left wheel is

The coordinate of the target XW wl, the coordinate of the center of gravity of the body XW , and the coordinate of the center of gravity of the fork XW are given by equations (2.3) to (2.7) , respectively . Here, let b be half the distance between the wheels .

$$XW_p = [xv, yv, R]^T \tag{2.3}$$

$$XW_{wr} = [xv + b \sin \ddot{y},\ yv \ddot{y} b \cos \ddot{y},\ R]^T \tag{2.4}$$

$$XW = [xv \ddot{y} b \sin \ddot{y},\ yv + b \cos \ddot{y},\ R]^T \quad \text{wl} \tag{2.5}$$

$$XW_b = \begin{bmatrix} \ddot{y}\ \ddot{y}\ xv + l\sin \ddot{y}p \cos \ddot{y} \\ yv + l\sin \ddot{y}p \sin \ddot{y} \\ R + l \cos \ddot{y}p \end{bmatrix} \tag{2.6}$$

$$XW_f = \begin{bmatrix} \ddot{y}\ \ddot{y}\ xv + L \sin \ddot{y}p \cos \ddot{y} + lf \cos \ddot{y}f\ddot{y}p \cos \ddot{y} \\ yv + L \sin \ddot{y}p \sin \ddot{y} + lf \cos \ddot{y}f\ddot{y}p \sin \ddot{y} \\ R + L \cos \ddot{y}p + lf \sin \ddot{y}f\ddot{y}p \end{bmatrix} \tag{2.7}$$

In addition, the rotation matrix RW from the world coordinate system to the vehicle coordinate system , and the rotation matrix RW from the world coordinate system to the body coordinate system

The rotation matrix RW from the world coordinate system to the fork coordinate system is given by equation (2.8),

(2.9) and equation (2.10) .

$$RW_v = \begin{bmatrix} \ddot{y}\ \ddot{y}\ \cos \ddot{y} \ddot{y} \sin \ddot{y} & 0 \\ \sin \ddot{y} \cos \ddot{y} & 0 \\ 0 & 0 \quad 1 \end{bmatrix} \tag{2.8}$$

$$RW_b = \begin{bmatrix} \ddot{y}\ \ddot{y}\ \ddot{y}\ \cos \ddot{y} \ddot{y} \sin \ddot{y} & 0 \\ \sin \ddot{y} \cos \ddot{y} & 0 \\ 0 \quad 0 & 1 \end{bmatrix} \begin{bmatrix} \ddot{y}\ \cos \ddot{y}p & 0 & \sin \ddot{y}p \\ 0 & 1 & 0 \\ \ddot{y} \sin \ddot{y}p & 0 & \cos \ddot{y}p \end{bmatrix}$$

$$= \begin{bmatrix} \ddot{y}\ \ddot{y}\ \cos \ddot{y} \cos \ddot{y}p & \ddot{y} \sin \ddot{y} & \cos \ddot{y} \sin \ddot{y}p \\ \sin \ddot{y} \cos \ddot{y}p & \cos \ddot{y} & \sin \ddot{y} \sin \ddot{y}p \\ \ddot{y} \sin \ddot{y}p & 0 & \cos \ddot{y}p \end{bmatrix} \tag{2.9}$$

$$RW_f = \begin{bmatrix} \ddot{y}\ \ddot{y}\ \ddot{y}\ \ddot{y}\ \cos \ddot{y} \cos \ddot{y}p & \ddot{y} \sin \ddot{y} & \cos \ddot{y} \sin \ddot{y}p \cos \ddot{y}f & 0 & \ddot{y} \sin \ddot{y}f \\ \sin \ddot{y} \cos \ddot{y}p & \cos \ddot{y} & \sin \ddot{y} \sin \ddot{y}p & 0 & \\ \ddot{y} \sin \ddot{y}p & 0 & \cos \ddot{y}p & 0 & 1 \\ & & & & \sin \ddot{y}f\ 0\ \cos \ddot{y}f \end{bmatrix}$$

$$= \begin{bmatrix} \ddot{y}\ \ddot{y}\ \cos \ddot{y} \cos(\ddot{y}p \ddot{y} \ddot{y}f) & \ddot{y} \sin \ddot{y} & \cos \ddot{y} \sin(\ddot{y}p \ddot{y} \ddot{y}f) \\ \sin \ddot{y} \cos(\ddot{y}p \ddot{y} \ddot{y}f) & \cos \ddot{y} & \sin \ddot{y} \sin(\ddot{y}p \ddot{y} \ddot{y}f) \\ \ddot{y} \sin(\ddot{y}p \ddot{y} \ddot{y}f) & 0 & \cos(\ddot{y}p \ddot{y} \ddot{y}f) \end{bmatrix} \tag{2.10}$$

The translational velocities of the centers of the left and right wheels, the center of mass of the body, and the center of mass of the fork are given by (2.4) to (2.7).

This can be derived by differentiating with respect to time, resulting in equation (2.14) from equation (2.11) .

$$Xÿ\ {}^{W}_{wr} = [\ \mathbf{xÿv} + bÿÿ\cos ÿ\ yÿv + bÿÿ\sin ÿ\ 0\ ]T = [\ \mathbf{xÿv} \tag{2.11}$$

$$Xÿ\ {}^{W}_{wl}\ \ ÿ\ bÿÿ\cos ÿ\ yÿv\ ÿ\ bÿÿ\sin ÿ\ 0\ ]T \tag{2.12}$$

$$Xÿ\ {}^{W}_{b} = \begin{matrix} \mathbf{ÿ}\ xÿv + lÿÿ_{p}\ \mathbf{ÿ}\cos ÿp\cos ÿ\ ÿ\ lÿÿ\sin ÿp\sin ÿ \\ yÿv + lÿÿ_{p}\cos ÿp\sin ÿ + lÿÿ\sin ÿp\cos ÿ \\ ÿlÿÿ_{p}\sin ÿp \end{matrix} \tag{2.13}$$

$$Xÿ\ Wf = \begin{matrix} \mathbf{ÿ}\ xÿv + Lÿÿ_{p}\cos ÿp\cos ÿ\ ÿ\ Lÿÿ\sin ÿp\sin ÿ\ ÿ\ lf\ ÿÿ\ fÿp\sin ÿfÿp\cos ÿ\ ÿ\ lf\ ÿÿ\cos ÿfÿp\sin ÿ\ \mathbf{ÿ} \\ yÿv + Lÿÿ_{p}\cos ÿp\sin ÿ + Lÿÿ\sin ÿp\cos ÿ\ ÿ\ lf\ ÿÿ\ fÿp\sin ÿfÿp\sin ÿ + lf\ ÿÿ\cos ÿfÿp\cos ÿ \\ ÿLÿÿ_{p}\sin ÿp + lf\ ÿÿ\ fÿp\cos ÿfÿp \end{matrix} \tag{2.14}$$

Next, the rotational angular velocity ÿ ${}^{W}_{b}$ is the body as seen from the world coordinate system

Using the rotation matrix RW to the coordinate system b, we obtain equation (2.15) .

$$\begin{aligned} Wÿb &= (Rÿ\ {}^{W}_{b}RWT_{b})^{ÿ} \\ &= \begin{matrix} ÿ & 0 & ÿÿÿ & ÿÿ_{p}\ \mathbf{ÿ}\cos ÿ^{ÿ} \\ & & 0 & ÿÿ_{p}\sin ÿ \\ -ÿÿÿ_{p}\ ÿÿ\cos ÿ & ÿÿÿ_{p}\sin ÿ & & 0 \end{matrix} \\ &= [\ \mathbf{ÿÿÿ}\ p\ \sin ÿ\ ÿÿ\ \ p\ \cos ÿ\ ÿÿ\ ]T \end{aligned} \tag{2.15}$$

Here, ÿ is the operation to extract a vector from a skew-symmetric matrix. Similarly, when viewed from the world coordinate system,

The angular velocity of rotation in the fork coordinate system is ÿ ${}^{W}_{f}$ is the rotation matrix RW f from the world coordinate system to the fork coordinate system

Using this we get equation (2.16) .

$$\begin{aligned} Wÿf &= (Rÿ\ {}^{W}_{f}RWT)_{f}^{V} \\ &= \begin{matrix} ÿ & & ÿÿÿ & ÿÿ\ \mathbf{ÿ}\ pÿf\cos ÿ^{ÿ} \\ & 0 & 0 & ÿÿ\ pÿf\sin ÿ \\ -ÿÿ\ ÿÿÿ\ pÿf\cos ÿ & ÿÿÿ\ pÿf\sin ÿ & & 0 \end{matrix} \\ &= [\ \mathbf{ÿÿÿ}\ pÿf\sin ÿ\ ÿÿ\ \ pÿf\cos ÿ\ ÿÿ\ ]T \end{aligned} \tag{2.16}$$

2.1.2 Constraints

In this section, we consider the constraints on the two-wheeled transport robot.

Since the body and the wheels are directly connected, the pitch angle, which is the inclination angle of the body relative to Zv in the vehicle coordinate system ÿv, is ÿp, and the rotational speeds of the left and right wheels relative to Zb in the body coordinate system ÿb are respectively

When ÿwbr and ÿwbl are taken as the origin, the rotational speeds of the left and right wheels as viewed from the vertical axis Zv with the center of the axle as the origin are ÿwr and ÿwl.

becomes equations (2.17) and (2.18) .

$$ÿwr = ÿwbr + ÿp \tag{2.17}$$

$$ÿwl = ÿwbl + ÿp \tag{2.18}$$

The rotational speeds ÿwr and ÿwl of each wheel as viewed from the vertical axis are obtained by time-differentiating equations (2.17) and (2.18) as follows:

(2.19) and equation (2.20) .

$$ÿwr = ÿÿwr = ÿÿwbr + ÿÿ_p \tag{2.19}$$

$$ÿwl = ÿÿwl = ÿÿwbl + ÿÿ_p \tag{2.20}$$

The rotational speeds of the wheels as viewed from the world coordinate system $\dot{ÿ}^{W}_{wr}$ are ÿ wr and $\dot{ÿ}^{W}_{wl}$ is the Yv axis of the vehicle coordinate system and the body coordinate system

Since the Yb axes of are the same, using equation (2.15) gives equations (2.21) and (2.22) , respectively.

$$\dot{ÿ}^{W}_{wr} = [\ ÿ(ÿÿwbr + ÿÿ\ p)\sin ÿ\ (ÿÿwbr + ÿÿ\ p)\cos ÿ\ ÿÿ\ ]T \tag{2.21}$$

$$Wÿwl = [\ ÿ(ÿÿwbl + ÿÿ\ p)\sin ÿ\ (ÿÿwbl + ÿÿ\ p)\cos ÿ\ ÿÿ\ ]T \tag{2.22}$$

In addition, the rotation angles ÿrr and ÿrl of the rotors of each wheel are expressed by the following equations (2.23), respectively, taking into account the reduction ratio of the gears.

This results in equation (2.24) , where nw is the gear ratio.

$$ÿrr = nwÿwbr + ÿp \tag{2.23}$$

$$ÿrl = nwÿwbl + ÿp \tag{2.24}$$

Similarly, the rotational angular velocities ÿrr and ÿrl of the rotors of each wheel viewed from the vertical axis are given by equations (2.25) and (2.26) , respectively.

Become.

$$ÿrr = nwÿÿwr = nwÿÿwbr + ÿÿ_p \tag{2.25}$$

$$ÿrl = nwÿÿwl = nwÿÿwbl + ÿÿ_p \tag{2.26}$$

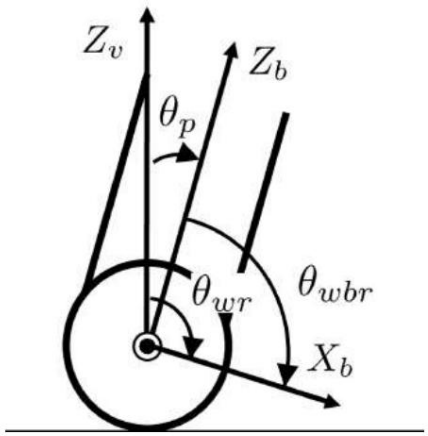

Fig. 2-3: Relationship between body and wheels

Rotor angular velocity ÿ as seen from the world coordinate system $^{W}_{rr,\ ÿrl}$ ^{W} Using equation (2.15) , equation (2.27) and equation (2.28) are obtained, respectively.

(2.28) .

$$ÿ\ ^{W}_{rr} = \mathbf{[\ ÿ}(nwÿÿwbr + ÿÿ\ p)\ \sin ÿ\ (nwÿÿwbr + ÿÿ\ p)\ \cos ÿ\ ÿÿ\ ]T = \tag{2.27}$$

$$W_{ÿrl}\quad \mathbf{[\ ÿ}(nwÿÿwbl + ÿÿ\ p)\ \sin ÿ\ (nwÿÿwbl + ÿÿ\ p)\ \cos ÿ\ ÿÿ\ ]T \tag{2.28}$$

Similarly, the angular velocity of the rotor attached to the fork , ÿ $^{W}_{rf}$ is expressed as (2.29) . Here, nf is the

is the gear ratio of the

$$W_{ÿrf}\quad = \mathbf{[\ ÿ}(ÿÿ_{p}\ ÿ\ nf\ ÿÿ\ f)\ \sin ÿ\ (ÿÿ_{p}\ ÿ\ nf\ ÿÿ\ f)\ \cos ÿ\ ÿÿ\ ]T \tag{2.29}$$

In addition, when the translational speed of the two-wheeled mobile transport robot is v , the constraint that the wheels do not slip is

This can be expressed as equation (2.30) .

$$\begin{aligned} v &= xÿv \cos ÿ + yÿv \sin ÿ \\ &= R\ \frac{ÿÿwr + ÿÿwl}{2} \end{aligned} \tag{2.30}$$

Furthermore, the velocity constraint condition that prevents the robot from moving in the axial direction can be expressed as equation (2.31) .

$$x\ddot{y}v \sin \ddot{y} \ddot{y} y\ddot{y}v \cos \ddot{y} = 0 \quad (2.31)$$

In addition, the travelling speeds of the left and right wheels are expressed by equations (2.32) and (2.33) , respectively .

$$v + b\ddot{y}\ddot{y} = R\ddot{y}\dot{y}wr \quad (2.32)$$

$$v \ddot{y} b\ddot{y}\ddot{y} = R\ddot{y}\dot{y}wl \quad (2.33)$$

From the relations in (2.19), (2.20) , and (2.30), (2.32), and (2.33) , we obtain the velocity constraint equation (2.34), Equation (2.35) is obtained.

$$x\ddot{y}v \cos \ddot{y} + y\ddot{y}v \sin \ddot{y} + b\ddot{y}\ddot{y} \ddot{y} R(\ddot{y}\dot{y}wbr + \ddot{y}\ddot{y} p) = 0 \quad (2.34)$$

$$x\ddot{y}v \cos \ddot{y} + y\ddot{y}v \sin \ddot{y} \ddot{y} b\ddot{y}\ddot{y} \ddot{y} R(\ddot{y}\dot{y}wbl + \ddot{y}\ddot{y} p) = 0 \quad (2.35)$$

2.2 Dynamics

2.2.1 Energy and potential energy of a two-wheeled mobile transport robot

In this section, we derive the equation of motion using the Lagrangian method.

The kinetic energy and potential energy are derived. The energy to be derived is the translational kinetic energy KwrT, KwlT and the rotational kinetic energy KwrR, KwlR of the left and right wheels, and the rotors of the left and right wheels. The rotational kinetic energies KrrR and KrlR in the

The kinetic energy of the rotor is Kr f R, the translational kinetic energy of the fork is Kf T, the rotational kinetic energy of the fork is Kf R, the rotational kinetic energy of the rotor in the fork section is Kr f R, and the potential energy is Upb .

First, we derive the translational kinetic energy KwT of the wheel. The mass of each wheel is mw , and the wheel

The wheel mass matrix Mw is defined as equation (2.36) .

$$Mw = \begin{matrix} \ddot{y}\ddot{y} \\ \\ \\ \_ \end{matrix} \begin{matrix} mw & 0 & 0 \\ 0 & mw & 0 \\ 0 & 0 & mw \end{matrix} \begin{matrix} \\ \\ \\ \_ \end{matrix} \quad (2.36)$$

Using equation (2.36) , the translational kinetic energies KwrT and KwlT of the left and right wheels are given by equations (2.37) and (2.38) , respectively .

$$KwrT = \frac{1}{2}(X\ddot{y}^{W}_{wr})\,TMw(X\ddot{y}\,W_{wr})$$

$$= \frac{1}{2}mw(\ddot{y}x_v^2 + y\ddot{y}_v^2 + b^2{}_{\ddot{y}\ddot{y}}{}^2) + mwb(\ddot{y}xv\dot{y}\ddot{y}\cos\ddot{y} + y\ddot{y}v\dot{y}\ddot{y}\sin\ddot{y}) \quad (2.37)$$

$$KwlT = wl)\ \frac{1}{2}(X\ddot{y}^{W}_{w})\,TMw(X\ddot{y}\,W$$

$$= \frac{1}{2}mw(\ddot{y}x_v^2 + b^2{}_{v}{}^2 + y\ddot{y}_{\ddot{y}\ddot{y}}{}^2)\ \ddot{y}\ mwb(\ddot{y}xv\dot{y}\ddot{y}\cos\ddot{y} + y\ddot{y}v\dot{y}\ddot{y}\sin\ddot{y}) \quad (2.38)$$

Next, calculate the rotational kinetic energy KwR of the wheel . In the vehicle coordinate system, when the wheel rotates,

The inertia tensor around the center of the wheel is defined as equation (2.39) .

$$I^{V}_{w} = \begin{bmatrix} \ddot{y}Iwx & 0 & 0 \\ 0 & Iwy & 0 \\ 0 & 0 & Iwz \end{bmatrix} \quad (2.39)$$

where Iwx, Iwy, and Iwz are the moments of inertia around the coordinate axes of the vehicle coordinate system ÿv . The inertia tensor I

$^{W}_{w}$ is calculated using the $_{v}$ rotation matrix RW as shown in equation (2.40) .

$$I^{W}_{w} = (RW_{v})I^{V}_{w}(RW_{v})^{T}$$

$$= \begin{bmatrix} \ddot{y}Iwx\cos2\ddot{y} + Iwy\sin2\ddot{y} & (Iwx\ddot{y}Iwy)\sin\ddot{y}\cos\ddot{y} & 0\ \ddot{y} \\ (Iwx\ddot{y}Iwy)\sin\ddot{y}\cos\ddot{y} & Iwx\sin2\ddot{y} + Iwy\cos2\ddot{y} & 0 \\ 0 & 0 & Iwz \end{bmatrix} \quad (2.40)$$

From equation (2.40) , the rotational kinetic energies KwrR and KwlR of the left and right wheels are given by equations (2.41) and (2.42) , respectively .

$$KwrR = \frac{1}{2}(\ddot{y}^{W}_{wr})^{T} I^{W}_{w}(\ddot{y}^{W}_{wr})$$

$$= \frac{1}{2}Iwy(\ddot{y}\dot{y}wbr + \ddot{y}\dot{y}p)^2 + \frac{1}{2}Iwz\ddot{y}\ddot{y}^2 \quad (2.41)$$

$$KwlR = (\ddot{y}^{W}_{wl})\,\frac{1}{2}{}^{T} I^{W}_{w}(\ddot{y}^{W}_{wl})$$

$$= \frac{1}{2}Iwy(\ddot{y}\dot{y}wbl + \ddot{y}\dot{y}p)^2 + \frac{1}{2}Iwz\ddot{y}\ddot{y}^2 \quad (2.42)$$

Similarly, calculate the rotational kinetic energy of the rotor of the wheel. The inertia of the rotor in the vehicle coordinate system is

Tensor I^{V}_{r} is shown in equation (2.43) .

$$I_r^V = \begin{bmatrix} Irx & 0 & 0 \\ 0 & Iry & 0 \\ 0 & 0 & Irz \end{bmatrix} \tag{2.43}$$

where Iwx, Iwy, and Iwz are the moments of inertia around the coordinate axes of the vehicle coordinate system ÿv . The rotational kinetic energies KrrR and KrlR of the left and right rotors are shown in equations (2.44) and (2.45) , respectively .

$$KrrR = \frac{1}{2}(\ddot{y}_{rr}^W)^T (R_b^W)^T I_r^V (R_b^W)(\ddot{y}_{rr}^W)$$
$$= \frac{1}{2} Iry(nw\ddot{y}wbr + \ddot{y}p)^2 + \frac{1}{2} Irz\ddot{y}^2 \tag{2.44}$$

$$KrlR = (\ddot{y}_{rl}^W)^T (R_b^W)^T I_r^V (R_b^W)(\ddot{y}_{rl}^W)$$
$$= \frac{1}{2} Iry(nw\ddot{y}wbl + \ddot{y}p)^2 + \frac{1}{2} Irz\ddot{y}^2 \tag{2.45}$$

Next, calculate the translational kinetic energy KbT of the body. The mass of the body is mb , and the wheel mass matrix Mb is

This is defined as equation (2.46) .

$$Mb = \begin{bmatrix} mb & 0 & 0 \\ 0 & mb & 0 \\ 0 & 0 & mb \end{bmatrix} \tag{2.46}$$

Using equation (2.46), the translational kinetic energy KbT of the body is given by equation (2.47) .

$$KbT = \frac{1}{2}(X\ddot{y}_b^W)^T Mb(X\ddot{y}_b^W)$$
$$= \frac{1}{2} mb(\ddot{y}x_v^2 + y\ddot{y}_v^2 + I^2\ddot{y}_p^2 + I^2\ddot{y}^2 \sin 2\ddot{y}p) + mbl\ddot{y}_p \cos \ddot{y}p(\ddot{y}xv \cos \ddot{y} + y\ddot{y}v \sin \ddot{y})$$
$$+ mbl\ddot{y}_p \sin \ddot{y}p(\ddot{y}x\ddot{y}v \sin \ddot{y} + y\ddot{y}v \cos \ddot{y}) \tag{2.47}$$

Next, we calculate the rotational kinetic energy KbR of the body . In the body coordinate system, the body rotates as

Inertia tensor I around the center of the wheel I_b^V is defined as equation (2.48) .

$$I_b^V = \begin{bmatrix} Ixx & 0 & 0 \\ 0 & Iyy & 0 \\ 0 & 0 & Izz \end{bmatrix} \tag{2.48}$$

Here, Ixx, Iyy, and Izz are the moments of inertia around the coordinate axes of the body coordinate system ÿv .

Inertia tensor I in the world coordinate system I_b^W is calculated using the rotation matrix RW as shown in equation (2.49) .

$$I_b^W = (RW_b)\, I_b\, (RW_b)^T = \begin{pmatrix} Ib11 & Ib12 & Ib13 \\ Ib21 & Ib22 & Ib23 \\ Ib31 & Ib32 & Ib33 \end{pmatrix} \tag{2.49}$$

Here, each element in equation (2.49) is shown in equations (2.50) to (2.55) .

$$Ib11 = Ixx \cos^2 ÿ \cos^2 ÿp + Iyy \sin^2 ÿ + Izz \cos^2 ÿ \sin^2 ÿp \tag{2.50}$$

$$Ib12 = Ib21 = (Ixx \cos^2 ÿp\, ÿ\, Iyy + Izz \sin^2 ÿp) \sin ÿ \cos ÿ \tag{2.51}$$

$$Ib13 = Ib31 = (ÿIxx + Izz) \cos ÿ \sin ÿp \cos ÿp \tag{2.52}$$

$$Ib22 = Ixx \sin^2 ÿ \cos^2 ÿp + Iyy \cos^2 ÿ + Izz \sin^2 ÿ \sin^2 ÿp \tag{2.53}$$

$$Ib23 = Ib32 = (ÿIxx + Izz) \sin ÿ \sin ÿp \cos ÿp \tag{2.54}$$

$$Ib33 = Ixx \sin^2 ÿp + Izz \cos^2 ÿp \tag{2.55}$$

From equation (2.49) , the rotational kinetic energy KbR of the body is given by equation (2.56) .

$$KbR = \frac{1}{2}(ÿ_b^W)^T I_b^W (ÿ_{wr}^W) = \frac{1}{2} Ixxÿÿ^2 \sin^2 ÿp + \frac{1}{2} Iyyÿÿ_p^2 + \frac{1}{2} Izzÿÿ^2 \cos^2 ÿp \tag{2.56}$$

As with the body, calculate the translational kinetic energy KfT and rotational kinetic energy KfR of the fork, and the rotational kinetic energy KfrR of the rotor in the fork section .

First, find the translational kinetic energy of the fork, Kf T. With the mass of the fork being mf , define the fork mass matrix Mf as equation (2.57) .

$$Mf = \begin{pmatrix} ÿ & ÿ & mf & 0 & 0 \\ & & 0 & mf & 0 \\ & & 0 & 0 & mf \end{pmatrix} \tag{2.57}$$

Using equation (2.57), the translational kinetic energy Kf T of the fork is given by equation (2.58) .

$$\begin{aligned} Kf\,T &= \frac{1}{2}(X\dot{y}_f^W)^T Mf(X\dot{y}_f^W) \\ &= \frac{1}{2}mf(\dot{y}x_v^2 + \dot{y}y_v^2 + L^2\dot{y}\dot{y}_p^2 + l_f^2\dot{y}\dot{y}_{fyp}^2 + L^2\dot{y}\dot{y}2\sin 2\dot{y}p + l_f^2\dot{y}\dot{y}2\cos 2\dot{y}f\dot{y}p) \\ &\quad + mf\{L\dot{y}\dot{y}\,p\cos\dot{y}p(\dot{y}xv\cos\dot{y} + y\dot{y}v\sin\dot{y}) + L\dot{y}\dot{y}\sin\dot{y}p(\dot{y}x\dot{y}v\sin\dot{y} + y\dot{y}v\cos\dot{y}) + lf\,\dot{y}\dot{y} \\ &\quad \cos\dot{y}f\dot{y}p(\dot{y}x\,\dot{y}v\sin\dot{y} + y\dot{y}v\cos\dot{y})\,\dot{y}\,lf\,\dot{y}\dot{y}\,f\dot{y}p\sin\dot{y}f\dot{y}p(\,\dot{y}xv\cos\dot{y} + y\dot{y}v\sin\dot{y}) \\ &\quad + LIf(\dot{y}\dot{y}^{\,2}\sin\dot{y}p\cos\dot{y}f\dot{y}p\,\dot{y}\,\dot{y}\dot{y}\,p\dot{y}\dot{y}\,f\dot{y}p\sin\dot{y}f)\} \end{aligned} \tag{2.58}$$

Next, we calculate the rotational kinetic energy Kf R of the fork.

Inertia tensor I f around the center of the fork when rotating ^{V} is defined as equation (2.59) .

$$If^V = \begin{matrix} \dot{y} \\ \dot{y} \\ \dot{y} \end{matrix}\begin{bmatrix} If\,x & \dot{y}\,0 & 0 \\ 0 & If\,y & 0 \\ 0 & 0 & If\,z \end{bmatrix} \tag{2.59}$$

tensor I f in the world is the moment of inertia around the coordinate axis of the fork coordinate system ÿf . Therefore, the inertia coordinate system of the fork is ^{W} is the rotation matrix Rv f Using this, we obtain equation (2.60) .

$$\begin{aligned} If^W &= (RW_f)I_f^V(RW_f)^T \\ &= \begin{matrix} \dot{y} \\ \dot{y} \\ \dot{y} \end{matrix}\begin{bmatrix} If\,11 & If\,12 & If\,13 \\ If\,21 & If\,22 & If\,23 \\ If\,31 & If\,32 & If\,33 \end{bmatrix} \end{aligned} \tag{2.60}$$

Each element in equation (2.60) is shown in equations (2.61) to (2.66) .

$$If\,11 = If\,x\ \cos2\,\dot{y}\cos2\,\dot{y}p\dot{y}f + If\,y\sin2\,\dot{y} + If\,z\cos2\,\dot{y}\sin2\,\dot{y}p\dot{y}f \tag{2.61}$$

$$If\,12 = If\,21 = (If\,x - If\,y)\cos\dot{y}\sin\dot{y}p\dot{y}f\cos\dot{y}p\dot{y}f - (If\,x - If\,y\sin2\,\dot{y}p\dot{y}f)\sin\dot{y} + If\,z\cos\dot{y} \tag{2.62}$$

$$If\,13 = If\,31 = (\dot{y}If\,x + If\,z)\cos\dot{y}\sin\dot{y}p\dot{y}f\cos\dot{y}p\dot{y}f \tag{2.63}$$

$$If\,22 = If\,x\ \sin2\,\dot{y}\cos2\,\dot{y}p\dot{y}f + If\,y\cos2\,\dot{y} + If\,z\sin2\,\dot{y}\sin2\,\dot{y}p\dot{y}f \tag{2.64}$$

$$If\,23 = If\,32 = (\dot{y}If\,x + If\,z)\sin\dot{y}\sin\dot{y}p\dot{y}f\cos\dot{y}p\dot{y}f \tag{2.65}$$

$$If\,33 = If\,x\ \sin2\,\dot{y}p\dot{y}f + If\,z\cos2\,\dot{y}p\dot{y}f \tag{2.66}$$

From equation (2.60) , the rotational kinetic energy of the fork, Kf R, is given by equation (2.67) .

$$\begin{aligned} Kf\,R &= \frac{1}{2}(\dot{y}_f^W)^T If^W(\dot{y}\,f^W) \\ &= \frac{1}{2}If\,x\dot{y}\dot{y}2\sin2\,\dot{y}p\dot{y}f + \frac{1}{2}If\,y\dot{y}\dot{y}_{p\dot{y}f}^2 + \frac{1}{2}If\,z\dot{y}\dot{y}2\cos2\,\dot{y}p\dot{y}f \end{aligned} \tag{2.67}$$

Similarly, calculate the rotational kinetic energy of the rotor in the fork. Rotor in the fork coordinate system

Inertia tensor I rf of f is shown in equation (2.68) .

$$I_{fr}^{f} = \begin{bmatrix} If\,rx & 0 & 0 \\ 0 & If\,ry & 0 \\ 0 & 0 & If\,rz \end{bmatrix} \quad (2.68)$$

energy , If rx, If ry, and If rz, is is the moment of inertia around the coordinate axis of the fork coordinate system ÿf . The rotor's rotational kinetic shown in equation (2.69) .

$$\begin{aligned} KrfR &= \tfrac{1}{2}(\ddot{y}_{f\,r})^{T}\,((RW_{f})I_{f\,r}(RW_{V}))^{T}(\ddot{y}_{f\,r}) \\ &= \frac{1}{2}If\,rx\ddot{y}^{2}\sin^{2}(\ddot{y}p\,\ddot{y}\,nf\,\ddot{y}f) + \frac{1}{2}If\,ry(\ddot{y}\ddot{y}\,p\,\ddot{y}\,nf\,\ddot{y}\ddot{y}\,f)^{2} + \frac{1}{2}If\,rz\ddot{y}\ddot{y}^{2}\cos^{2}(\ddot{y}p\,\ddot{y}\,nf\,\ddot{y}f) \end{aligned} \quad (2.69)$$

From the above, the total kinetic energy Kp of the robot is given by equation (2.70) .

$$Kp = KwrT + KwlT + KwrR + KwlR + KrrR + KrlR + KbT + KbR + Kf\,T + Kf\,R + Kr\,f\,R \quad (2.70)$$

Finally, we calculate the potential energy Upb of the two-wheeled mobile transport robot . The robot moves on a horizontal plane. When the rotor axis is aligned with the wheel axis, the potential energy due to the wheel weight is

Therefore, the potential energy Upb can be calculated from the gravity acting on the center of gravity of the body and the center of gravity of the fork, as given by equation (2.71) from equations (2.6) and (2.7) .

$$Upb = mb(R + l\cos\ddot{y}p)g + mf(R + L\cos\ddot{y}p + lf\sin\ddot{y}f\ddot{y}p)g \quad (2.71)$$

From equations (2.70) and (2.71) , the Lagrangian Lp is given by equation (2.72) .

$$
\begin{aligned}
Lp &= Kp \ddot{y} Upb \\
&= mw(\dot{y}x_v^2 + y\ddot{y}_v^2 + b^2 \ddot{y}_{\ddot{y}}^2) + \frac{1}{2} Iwy(\ddot{y}\ddot{y}wbr + \ddot{y}\ddot{y}p)^2 + \frac{1}{2} Iwy(\ddot{y}\ddot{y}wbl + \ddot{y}\ddot{y}p)^2 + Iwz\ddot{y}\ddot{y}^2 \\
&+ \frac{1}{2} Iry(nw\ddot{y}\ddot{y}wbr + \ddot{y}\ddot{y}p)^2 + \frac{1}{2} Iry(nw\ddot{y}\ddot{y}wbl + \ddot{y}\ddot{y}p)^2 + Irz\ddot{y}\ddot{y}^2 \\
&+ \frac{1}{2} mb(\dot{y}x_v^2 + y\ddot{y}_v^2 + l^2 \ddot{y}_{\ddot{y}p}^2 + l^2 \ddot{y}\ddot{y}2 \sin 2 \ddot{y}p) + mbl\ddot{y}\ddot{y}_p \cos \ddot{y}p(\dot{y}xv \cos \ddot{y} + y\ddot{y}v \sin \ddot{y}) \\
&+ mbl\ddot{y}\ddot{y}_p \sin \ddot{y}p(\dot{y}x\ddot{y}v \sin \ddot{y} + y\ddot{y}v \cos \ddot{y}) + \frac{1}{2} Ixy\ddot{y}2 \sin 2 \ddot{y}p + \frac{1}{2} Iyy\ddot{y}\ddot{y}_p^2 + \frac{1}{2} Izy\ddot{y}2 \cos 2 \ddot{y}p \\
&+ \frac{1}{2} mf(\dot{y}x_v^2 + y\ddot{y}_v^2 + L^2 l f_{p\ddot{y}}^2 \ddot{y}\ddot{y} + L^2 f\ddot{y}_p^2 \ddot{y}\ddot{y} + L^2 l f\ddot{y}\ddot{y}2 \sin 2 \ddot{y}p + l^2 \ddot{y}\ddot{y}_f^2 \ddot{y}\ddot{y}2 \cos 2 \ddot{y}f\ddot{y}p) \\
&+ mf\{L\ddot{y}\ddot{y}_p \cos \ddot{y}p(\dot{y}xv \cos \ddot{y} + y\ddot{y}v \sin \ddot{y}) + L\ddot{y}\ddot{y} \sin \ddot{y}p(\dot{y}x\ddot{y}v \sin \ddot{y} + y\ddot{y}v \cos \ddot{y})\} \\
&+ mf\{lf \ddot{y}\ddot{y} \cos \ddot{y}f\ddot{y}p(\dot{y}x\ddot{y}v \sin \ddot{y} + y\ddot{y}v \cos \ddot{y}) \ddot{y} lf \ddot{y}\ddot{y} f\ddot{y}p \sin \ddot{y}f\ddot{y}p(\dot{y}xv \cos \ddot{y} + y\ddot{y}v \sin \ddot{y})\} \\
&+ mf\{Llf(\ddot{y}\ddot{y}^2 \sin \ddot{y}p \cos \ddot{y}f\ddot{y}p \ddot{y} \ddot{y}\ddot{y} p\ddot{y}\ddot{y} f\ddot{y}p \sin \ddot{y}f)\} \\
&+ \frac{1}{twenty} lf x\ddot{y}\ddot{y}2 \sin 2 \ddot{y}p\ddot{y}f + \frac{1}{2} lf y\ddot{y}\ddot{y}_{p\ddot{y}f}^2 + \frac{1}{2} lf z\ddot{y}\ddot{y}2 \cos 2 \ddot{y}p\ddot{y}f \\
&+ \frac{1}{2} lf rx\ddot{y}\ddot{y}2 \sin 2 (\ddot{y}p \ddot{y} nf \ddot{y}f) + \frac{1}{2} lf ry(\ddot{y}\ddot{y} p \ddot{y} nf \ddot{y}\ddot{y} f)^2 + \frac{1}{2} lf rz\ddot{y}\ddot{y}2 \cos 2 (\ddot{y}p \ddot{y} nf \ddot{y}f) \\
&\ddot{y} mb(R + l \cos \ddot{y}p)g \ddot{y} mf(R + L \cos \ddot{y}p + lf \sin \ddot{y}f\ddot{y}p)g
\end{aligned}
\tag{2.72}
$$

2.2.2 Equation of motion before considering constraint conditions

In this subsection, we use the Lagrangian method to obtain the dynamics of a two-wheeled mobile transport robot without constraints. We derive the equation of motion of the two-wheeled mobile transport robot by substituting the Lagrangian Lp derived in the previous subsection into the Lagrangian equation in equation (2.73) .

$$
\frac{d}{dt}\left(\frac{\ddot{y}L}{\ddot{y}\dot{q}i}\right) \ddot{y} \frac{\ddot{y}L}{\ddot{y}qi} = Qi \tag{2.73}
$$

Here, q represents the generalized coordinate defined by equation (2.74) , and Q represents the generalized force. i represents the degree of freedom, and q and Q indicate the elements corresponding to each degree of freedom.

$$
q = [\, xv \; yv \; \ddot{y} \; \ddot{y}wbr \; \ddot{y}wbl \; \ddot{y}p \; \ddot{y}f \,]^T \tag{2.74}
$$

First, consider the generalized force Q, which is the right-hand side of the Lagrange equation.

In this model, the generalized force is generated by the motors connected to the left and right wheels and the fork, and the work W is expressed by the formula: (2.75) where the driving torques of the left and right wheel motors are ÿr and ÿl, and the driving torque of the fork motor is

Let k be ÿf .

$$W = \text{ÿwbrnwÿr} + \text{ÿwblnwÿl} + \text{ÿf nf ÿf} \tag{2.75}$$

The generalized force Q is expressed by equation (2.76) . Also, E and the vector ÿ representing the motor drive torque are expressed by

These are shown in equations (2.77) and (2.78) , respectively .

$$Q = \begin{matrix} \text{ÿ} \\ \\ \\ \\ \\ \\ \\ \\ \text{ÿ} \end{matrix} \begin{bmatrix} 0 & 0 & \text{ÿ}\,0 \\ 0 & 0 & 0 \\ 0 & 0 & 0 \\ \frac{\text{ÿW}}{\text{ÿÿwbr}} & 0 & 0 \\ 0 & \frac{\text{ÿW}}{\text{ÿÿwbl}} & 0 \\ 0 & 0 & 0 \\ 0 & 0 & \frac{\text{ÿW}}{\text{ÿÿ f}} \end{bmatrix} \begin{matrix} \text{ÿ} \\ \\ \\ \\ \\ \\ \\ \\ \text{ÿ} \end{matrix}$$

$$= \begin{matrix} \text{ÿ} \\ \\ \\ \\ \\ \\ \\ \\ \text{ÿ} \end{matrix} \begin{bmatrix} 0\,0\,0 \\ 0\,0\,0 \\ 0\,0\,0 \\ \text{nw}\,0\,0 \\ 0\text{n}0 \\ 0\,0\,0 \\ 0\,0\,\text{nf} \end{bmatrix} \begin{matrix} \\ \\ \\ \text{ÿ ÿr ÿ} \\ \text{ÿl} \\ \text{ÿf} \\ \\ \\ \end{matrix}$$

$$= E\text{ÿ} \tag{2.76}$$

$$E = \begin{matrix} \text{ÿ} \\ \\ \\ \\ \\ \\ \\ \\ \text{ÿ} \end{matrix} \begin{bmatrix} 0\,0\,0\,\text{nw}\,0\,0\,0 \\ 0\,0\,0\,0\,\text{nw}\,0\,0 \\ 0\,0\,0\,0\,0\,0\,\text{nf} \end{bmatrix}^{\text{T}} \begin{matrix} \\ \\ \\ \text{ÿ} \\ \\ \\ \\ \\ \end{matrix} \tag{2.77}$$

$$\text{ÿ} = [\ \text{ÿr ÿl ÿf}\ ]^{\text{T}} \tag{2.78}$$

We solve the Lagrangian equation from the Lagrangian Lp in equation (2.72) and the generalized force in equation (2.76) . First, The Lagrange equation for xv is given by equation (2.79) .

$$\frac{d}{dt}\left(\frac{\text{ÿL}}{\text{ÿ}\dot{x}\text{v}}\right) - \frac{\text{ÿL}}{\text{ÿxv}} = 0 \tag{2.79}$$

By calculating each element of equation (2.79) , equation (2.82) can be obtained from equation (2.80) .

$$\frac{\partial L}{\partial \dot{x}_v} = (2m_w + m_b + m_f)\,\dot{x}_v + \dot{\psi}\dot{x}_v$$

$$+ m_b l(\ddot{\psi}_p \cos\psi_p \cos\psi + \dot{\psi}\dot{\psi}_p \sin\psi_p \sin\psi) + m_f L(\ddot{\psi}_p \cos\psi_p \cos\psi + \dot{\psi}\dot{\psi}_p \sin\psi_p \sin\psi)$$

$$+ m_f l_f(\ddot{\psi}\cos\psi_{fp} \sin\psi_p \cos\psi + \dot{\psi}\dot{\psi}_p \cos\psi_{fp} \cos\psi) \tag{2.80}$$

$$\frac{d}{dt}\left(\frac{\partial L}{\partial \dot{x}_v}\right) = (2m_w + m_b + m_f)\,\ddot{x}_v + (m_b l + m_f L)(\ddot{\psi} \cos\psi_p \cos\psi - \dot{\psi}\dot{\psi}_p \sin\psi_p \cos\psi)$$

$$+ (m_b l + m_f L)(-2\dot{\psi}\dot{\psi}_p \sin\psi_p \cos\psi - \dot{\psi}^2 \sin\psi_p \cos\psi)$$

$$+ m_f l_f(\ddot{\psi}\cos\psi_{fp} \sin\psi_p \cos\psi - \dot{\psi}\dot{\psi}_p \cos\psi_{fp} \cos\psi)$$

$$+ m_f l_f(-2\dot{\psi}\dot{\psi}_{fp} \sin\psi_{fp} \sin\psi + \ddot{\psi} \cos\psi_{fp} \sin\psi - \dot{\psi}^2 \cos\psi_{fp} \cos\psi) \tag{2.81}$$

$$\frac{\partial L}{\partial x_v} = 0 \tag{2.82}$$

From equations (2.81) and (2.82) , the equation of motion for xv is shown in equation (2.83) .

$$(2m_w + m_b + m_f)\,\ddot{x}_v + (m_b l + m_f L)(\ddot{\psi} \cos\psi_p \cos\psi - \dot{\psi}\dot{\psi}_p \sin\psi_p \cos\psi)$$

$$+ (m_b l + m_f L)(-2\dot{\psi}\dot{\psi}_p \sin\psi_p \cos\psi - \dot{\psi}^2 \sin\psi_p \cos\psi)$$

$$+ m_f l_f(\ddot{\psi}\cos\psi_{fp} \sin\psi_p \cos\psi - \dot{\psi}\dot{\psi}_p \cos\psi_{fp} \cos\psi)$$

$$+ m_f l_f(-2\dot{\psi}\dot{\psi}_{fp} \sin\psi_{fp} \sin\psi + \ddot{\psi} \cos\psi_{fp} \sin\psi - \dot{\psi}^2 \cos\psi_{fp} \cos\psi) = 0 \tag{2.83}$$

Next, the Lagrange equation for yv is given by equation (2.84) .

$$\frac{d}{dt}\left(\frac{\partial L}{\partial \dot{y}_v}\right) - \frac{\partial L}{\partial y_v} = 0 \tag{2.84}$$

By calculating each element of equation (2.84) , equation (2.87) can be obtained from equation (2.85) .

$$\frac{\partial L}{\partial \dot{y}_v} = (2m_w + m_b + m_f)\dot{y}_v + m_b l(\ddot{\psi}_p \cos\psi_p \sin\psi + \dot{\psi}\dot{\psi}_p \sin\psi_p \cos\psi)$$

$$+ m_f L(\ddot{\psi}_p \cos\psi_p \sin\psi + \dot{\psi}\dot{\psi}_p \sin\psi_p \cos\psi)$$

$$+ m_f l_f(\ddot{\psi}\dot{\psi}_{fp} \sin\psi_{fp} \sin\psi + \dot{\psi}\dot{\psi}_{fp} \cos\psi_{fp} \cos\psi) \tag{2.85}$$

$$\frac{d}{dt}\left(\frac{\partial L}{\partial \dot{y}_v}\right) = (2m_w + m_b + m_f)\ddot{y}_v + (m_b l + m_f L)(\ddot{\psi} \cos\psi_p \sin\psi + \dot{\psi}\dot{\psi}_p \sin\psi_p \sin\psi)$$

$$+ (m_b l + m_f L)(2\dot{\psi}\dot{\psi}_p \cos\psi_p \cos\psi + \ddot{\psi} \sin\psi_p \cos\psi - \dot{\psi}^2 \sin\psi_p \sin\psi)$$

$$+ m_f l_f(\ddot{\psi}\cos\psi_{fp} \sin\psi_{fp} \sin\psi + \dot{\psi}\dot{\psi}_{fp} \cos\psi_{fp} \sin\psi)$$

$$+ m_f l_f(-2\dot{\psi}\dot{\psi}_{fp} \sin\psi_{fp} \cos\psi + \ddot{\psi} \cos\psi_{fp} \cos\psi - \dot{\psi}^2 \cos\psi_{fp} \sin\psi) \tag{2.86}$$

$$\frac{\partial L}{\partial y_v} = 0 \tag{2.87}$$

From equations (2.86) and (2.87) , the equation of motion for yv is shown in equation (2.88) .

$$(2mw + mb + mf)\ddot{y}v + (mbl + mf L)(\ddot{y}\ \ p\cos\ddot{y}p\sin\ddot{y}\,\ddot{y}\ddot{y}\ {}^{2}_{p}\sin\ddot{y}p\sin\ddot{y})$$
$$+ (mbl + mf L)(2\ddot{y}\ddot{y}\ p\ddot{y}\ddot{y}\cos\ddot{y}p\cos\ddot{y}\,\ddot{y}\,\ddot{y}\ddot{y} + \ {}^{2}\sin\ddot{y}p\sin\ddot{y})$$
$$mf\,lf(\ddot{y}\ddot{y}\ddot{y}\ f\ddot{y}p\sin\ddot{y}f\ddot{y}p\sin\ddot{y}\,\ddot{y}\,\ddot{y}\ddot{y}\ \ {}^{2}_{f\ddot{y}p}\cos\ddot{y}f\ddot{y}p\sin\ddot{y})$$
$$+ mf\,lf(\ddot{y}2\ddot{y}\ddot{y}\ f\ddot{y}p\ddot{y}\ddot{y}\sin\ddot{y}f\ddot{y}p\cos\ddot{y} + \ddot{y}\ddot{y}\cos\ddot{y}f\ddot{y}p\cos\ddot{y}\,\ddot{y}\,\ddot{y}\ddot{y}\ \ {}^{2}\cos\ddot{y}f\ddot{y}p\sin\ddot{y}) = 0 \quad (2.88)$$

Next, the Lagrange equation for ÿ is given by equation (2.89) .

$$\frac{d}{dt}\left(\frac{\ddot{y}L}{\ddot{y}\ddot{y}}\right) - \frac{\ddot{y}L}{\ddot{y}\ddot{y}} = 0\ \ddot{y}\ddot{y} \quad (2.89)$$

By calculating each element of equation (2.89) , equation (2.92) can be obtained from equation (2.90) .

$$\frac{\ddot{y}L2}{} = 2mwb\ \ddot{y}\ddot{y}\ddot{y}\ \ddot{y}\ddot{y}\,v + 2\ddot{y}\ddot{y}(Iwz + Irz) + mbl\ {}^{2}\ddot{y}\ddot{y}\sin2\ddot{y}p + (mbl + mf L)\sin\ddot{y}p(\ddot{y}x\ddot{y}v\sin\ddot{y} + y\ddot{y}v\cos\ddot{y})$$
$$+ Ixx\ddot{y}\ddot{y}\sin2\ddot{y}p + Izz\ddot{y}\ddot{y}\cos2\ddot{y}p + mf\,\ddot{y}\ddot{y}(L\sin\ddot{y}p + lf\cos\ddot{y}f\ddot{y}p)\ {}^{2}$$
$$+ mf\,lf\cos\ddot{y}f\ddot{y}p(\ddot{y}x\ddot{y}v\sin\ddot{y} + y\ddot{y}v\cos\ddot{y}) + 2mf\,lf\,L\ddot{y}\ddot{y}\sin\ddot{y}p\cos\ddot{y}f\ddot{y}p + lf\,x\ddot{y}\ddot{y}$$
$$\sin2\ddot{y}p\ddot{y}f + lf\,z\ddot{y}\ddot{y}\cos2\ddot{y}p\ddot{y}f + lf\,rx\ddot{y}\ddot{y}\sin2(\ddot{y}p\,\ddot{y}\,nf\,\ddot{y}f) + lf\,rz\ddot{y}\ddot{y}\cos2(\ddot{y}p\,\ddot{y}\,nf\,\ddot{y}f) \quad (2.90)$$

$$\frac{d}{dt}\left(\frac{\ddot{y}L}{\ddot{y}\ddot{y}}\right) = (mblsin\ddot{y}p + mf\,L\sin\ddot{y}p + mf\,lf\cos\ddot{y}f\ddot{y}p)(\ddot{y}x\ddot{y}v\sin\ddot{y}\,\ddot{y}\,x\ddot{y}v\ddot{y}\ddot{y}\cos\ddot{y} + y\ddot{y}v\cos\ddot{y}\,\ddot{y}\,y\ddot{y}v\ddot{y}\ddot{y}\sin\ddot{y})$$
$$2 + (2mwb\ \ + 2Iwz + 2Irz + Ixx\sin2\ddot{y}p + lf\,x\sin2\ddot{y}p\ddot{y}f + lf\,rx\sin2(\ddot{y}p\,\ddot{y}\,nf\,\ddot{y}f))\ddot{y}\ddot{y}$$
$$+ (Izz\cos2\ddot{y}p + lf\,z\cos2\ddot{y}p\ddot{y}f + lf\,rz\cos2(\ddot{y}p\,\ddot{y}\,nf\,\ddot{y}f) + 2mf\,lf\,L\sin2\ddot{y}f)\ddot{y}\ddot{y}$$
$$+ (mbl\ddot{y}\ddot{y}_{p}\cos\ddot{y}p + mf\,L\ddot{y}\ddot{y}\ \ {}_{p}\cos\ddot{y}p\,\ddot{y}\,mf\,lf\,\ddot{y}\ddot{y}\,f\ddot{y}p\sin\ddot{y}f\ddot{y}p)(\ddot{y}x\ddot{y}v\sin\ddot{y} + y\ddot{y}v\cos\ddot{y})$$
$$+ (Ixx\ddot{y}\ddot{y}_{p}\sin2\ddot{y}p + lf\,x\ddot{y}\ddot{y}\,p\ddot{y}f\sin2\ddot{y}p\ddot{y}f + lf\,rx(\ddot{y}\ddot{y}\ \ {}_{p}\ \ddot{y}\,nf\,\ddot{y}\ddot{y}\,f)\sin2(\ddot{y}p\,\ddot{y}\,nf\,\ddot{y}f))\ddot{y}\ddot{y}$$
$$\ddot{y}\ (Izz\ddot{y}\ddot{y}_{p}\sin2\ddot{y}p + lf\,z\ddot{y}\ddot{y}\,p\ddot{y}f\sin2\ddot{y}p\ddot{y}f + lf\,rz(\ddot{y}\ddot{y}\ \ {}_{p}\ \ddot{y}\,nf\,\ddot{y}\ddot{y}\,f)\sin2(\ddot{y}p\,\ddot{y}\,nf\,\ddot{y}f))\ddot{y}\ddot{y}$$
$$+ 4mf\,lf\,L\ddot{y}\ddot{y}\ddot{y}\ddot{y}\,f\cos2\ddot{y}f \quad (2.91)$$

$$\frac{\ddot{y}L}{\ddot{y}\ddot{y}} = (mbl + mf L)\ddot{y}\ddot{y}\ \ {}_{p}\cos\ddot{y}p(\ddot{y}x\ddot{y}v\sin\ddot{y} + y\ddot{y}v\cos\ddot{y})$$
$$\ddot{y}\ (mbl + mf L)\ddot{y}\ddot{y}\sin\ddot{y}p(\ \ddot{y}xv\cos\ddot{y} + y\ddot{y}v\sin\ddot{y})$$
$$\ddot{y}\ mf\,lf\,\ddot{y}\ddot{y}\cos\ddot{y}f\ddot{y}p(\ \ddot{y}xv\cos\ddot{y} + y\ddot{y}v\sin\ddot{y}) + mf\,lf\,\ddot{y}\ddot{y}\,f\ddot{y}p\sin\ddot{y}f\ddot{y}p(\ \ddot{y}xv\sin\ddot{y}\,\ddot{y}\,y\ddot{y}v\cos\ddot{y}) \quad (2.92)$$

From equations (2.91) and (2.92) , the equation of motion for ÿ is shown in equation (2.93) .

(mblsin ÿp + mf L sin ÿp + mf lf cos ÿfÿp)(ÿx¨v sin ÿ ÿ xÿvÿÿ cos ÿ + y¨v cos ÿ ÿ yÿvÿÿ sin ÿ)

+ (2mwb 2 + 2Iwz + 2Irz + Ixx sin2 ÿp + If x sin2 ÿpÿf + If rx sin2 (ÿp ÿ nf ÿf))ÿ¨

+ (Izz cos2 ÿp + If z cos2 ÿpÿf + If rz cos2 (ÿp ÿ nf ÿf) + 2mf lf L sin 2ÿf)ÿ¨

+ (mblÿÿ p cosÿp + mf Lÿÿ p cos ÿp ÿ mf lf ÿÿ fÿp sin ÿfÿp)(ÿxÿv sin ÿ + yÿv cos ÿ)

+ (Ixxÿÿ p sin 2ÿp + If xÿÿ pÿf sin 2ÿpÿf + If rx(ÿÿ p ÿ nf ÿÿ f) sin 2(ÿp ÿ nf ÿf))ÿÿ

ÿ (Izzÿÿ p sin 2ÿp + If zÿÿ pÿf sin 2ÿpÿf + If rz(ÿÿ p ÿ nf ÿÿ f) sin 2(ÿp ÿ nf ÿf))ÿÿ

+ 4mf lf Lÿÿÿÿ f cos 2ÿf ÿ (mbl + mf L)ÿÿ p cos ÿp(ÿxÿv sin ÿ + yÿv cos ÿ)

+ (mbl + mf L)ÿÿ sin ÿp(ÿxv cos ÿ + yÿv sin ÿ)

+ mf lf ÿÿ cos ÿfÿp(ÿxv cos ÿ + yÿv sin ÿ) ÿ mf lf ÿÿ fÿp sin ÿfÿp(ÿxv sin ÿ ÿ yÿv cos ÿ) = 0 (2.93)

Next, the Lagrangian equation for ÿwbr is given by equation (2.94) .

d/dt (ÿL / ÿÿwbr) ÿ ÿL / ÿÿwbr = nwÿr (2.94)

By calculating each element of equation (2.94) , equation (2.97) can be obtained from equation (2.95) .

ÿL / ÿÿÿwbr =Iwy(ÿÿwbr + ÿÿ p) + Irynw(nwÿÿwbr + ÿÿ p) (2.95)

d/dt (ÿL / ÿÿwbr) =Iwy(ÿ¨wbr + ÿ¨ p) + Irynw(nwÿ¨wbr + ÿ¨ p) (2.96)

ÿL / ÿÿwbr =0 (2.97)

From equations (2.96) and (2.97) , the equation of motion for ÿwbr is shown in equation (2.98) .

Iwy(ÿ¨wbr + ÿ¨ p) + Irynw(nwÿ¨wbr + ÿ¨ p) = nwÿr (2.98)

Next, the Lagrangian equation for ÿwbl is given by equation (2.99) .

d/dt (ÿL / ÿÿÿwbl) ÿ ÿL / ÿÿwbl = nwÿl (2.99)

By calculating each element of equation (2.99) , equation (2.102) can be obtained from equation (2.100) .

ÿL / ÿÿÿwbl =Iwy(ÿÿwbl + ÿÿ p) + Irynw(nwÿÿwbl + ÿÿ p) (2.100)

d/dt (ÿL / ÿÿwbr) =Iwy(ÿ¨wbr + ÿ¨ p) + Irynw(nwÿ¨wbl + ÿ¨ p) (2.101)

ÿL / ÿÿwbr =0 (2.102)

From equations (2.101) and (2.102) , the equation of motion for ÿwbl is shown in equation (2.103) .

$$Iwy(ÿ¨wbl + ÿ¨\ p) + Irynw(nwÿ¨wbl + ÿ¨\ p) = nwÿl \tag{2.103}$$

Next, the Lagrange equation for ÿp is given by equation (2.104) .

$$\frac{d}{dt}\left(\frac{ÿL}{ÿÿÿ_p}\right) ÿ \frac{ÿL}{ÿÿp} = 0 \tag{2.104}$$

By calculating each element of equation (2.104) , equation (2.107) can be obtained from equation (2.105) .

$$\frac{ÿL}{ÿÿÿ_p} = Iwy(ÿÿwbr + ÿÿ\ p) + Iwy(ÿÿwbl + ÿÿ\ p) + Iry(nwÿÿwbr + ÿÿ\ p) + Iry(nwÿÿwbl + ÿÿ\ p)$$
$$+ (mbl^2 + Iyy + mf\ L^2)ÿÿ_p + (mbl\cos ÿp + mf\ L\cos ÿp + mf\ lf\sin ÿfÿp)(\ ÿxv\cos ÿ + yÿv\sin ÿ)$$
$$ÿÿ\ fÿp\ ÿ\ mf\ Llf\sin ÿf(ÿÿ\ f\ ÿ\ 2ÿÿ\ p) + If\ yÿÿ\ pÿf + If\ ry(ÿÿ\ p\ ÿ\ nf\ ÿÿ\ f)\ ÿ\ mf\ l\ f^2 \tag{2.105}$$

$$\frac{d}{dt}\left(\frac{ÿL}{ÿÿÿ_p}\right) = Iwy(ÿ¨wbr + ÿ¨\ p) + Iwy(ÿ¨wbl + ÿ¨\ p) + Iry(nwÿ¨wbr + ÿ¨\ p) + Iry(nwÿ¨wbl + ÿ¨\ p) + (mbl^2 + Iyy + mf\ L^2)ÿ¨_p$$
$$+ (ÿmblÿÿ_p\sin ÿp\ ÿ\ mf\ Lÿÿ_p\sin ÿp + mf\ lf\ ÿÿ\ fÿp\cos ÿfÿp)(\ ÿxv\cos ÿ + yÿv\sin ÿ)$$
$$+ (mbl\cos ÿp + mf\ L\cos ÿp + mf\ lf\sin ÿfÿp)(\ ¨xv\cos ÿ\ ÿ\ xÿvÿÿ\sin ÿ + y¨v\sin ÿ + yÿvÿÿ\cos ÿ)$$
$$ÿ\ mf\ l^2 ÿ¨\ fÿp\ ÿ\ mf\ Llf\cos ÿf(ÿÿ\ f\ ÿ\ 2ÿÿ\ p)ÿÿ\ f\ ÿ\ mf\ Llf\sin ÿf(ÿ¨\ f\ ÿ\ 2ÿ¨\ p)\ f$$
$$+ If\ yÿ¨\ pÿf + If\ ry(ÿ¨\ p\ ÿ\ nf\ ÿ¨\ f) \tag{2.106}$$

$$\frac{ÿL}{ÿÿp} = 2 mbl^2 ÿÿ^2\sin ÿp\cos ÿp\ ÿ\ mblÿÿ_p\sin ÿp(\ ÿxv\cos ÿ + yÿv\sin ÿ) + mblÿÿ_p\cos ÿp(ÿxÿv\sin ÿ + yÿv\cos ÿ)$$
$$+ Ix\ xÿÿ^2\sin ÿp\cos ÿp\ ÿ\ Izzÿÿ^2\sin ÿ\cos ÿ + mf(L^2_{ÿÿ}{}^2\sin ÿp\cos ÿp\ ÿ\ l^2_f{}_{ÿÿ}{}^2\sin ÿfÿp\cos ÿfÿp)$$
$$ÿ\ mf\ Lÿÿ_p\sin ÿp(\ ÿxv\cos ÿ + yÿv\sin ÿ) + mf\ Lÿÿ\cos ÿp(ÿxÿv\sin ÿ + yÿv\cos ÿ)$$
$$ÿ\ mf\ lf\ ÿÿ\sin ÿfÿp(ÿxÿv\sin ÿ + yÿv\cos ÿ) + mf\ lf\ ÿÿ\ fÿp\cos ÿfÿp(\ ÿxv\cos ÿ + yÿv\sin ÿ)$$
$$+ mf\ Llf\ ÿÿ^2\cos ÿf\ ÿ2p + If\ xÿÿ^2\sin ÿpÿf\cos ÿpÿf\ ÿ\ If\ zÿÿ^2\cos ÿpÿf\sin ÿpÿf$$
$$+ (If\ rx^2 ÿ\ If\ rz)ÿÿ^2\sin(ÿp\ ÿ\ nf\ ÿf)\cos(ÿp\ ÿ\ nf\ ÿf)$$
$$+ mblg\sin ÿp + mf\ gL\sin ÿp + mf\ glf\cos ÿfÿp \tag{2.107}$$

From equations (2.106) and (2.107) , the equation of motion for ÿp is shown in equation (2.108) .

$$
\begin{aligned}
&Iwy(\ddot{y}_{wbr} + \ddot{y}_p) + Iwy(\ddot{y}_{wbl} + \ddot{y}_p) + Iry(nw\ddot{y}_{wbr} + \ddot{y}_p) + Iry(nw\ddot{y}_{wbl} + \ddot{y}_p)\\
&+ (mbl^2 + Iyy + mf L^2)\ddot{y}_p + (\ddot{y}_{mblÿÿ_p}\sin ÿp\, ÿ\, mf L\ddot{y}_{ÿ_p}\sin ÿp + mf lf ÿÿ fÿp\cos ÿfÿp)(\ddot{x}_v\cos ÿ + ÿ\ddot{v}\sin ÿ)\\
&+ (mbl\cos ÿp + mf L\cos ÿp + mf lf\sin ÿfÿp)(\ddot{x}_v\cos ÿ\, ÿ\, x\ddot{y}_{vÿÿ}\sin ÿ + \ddot{y}_v\sin ÿ + ÿ\ddot{v}_{ÿÿ}\cos ÿ)\\
&ÿ\, mf l^2\ddot{y}_{fÿp}\, ÿ\, mf Llf\cos ÿf(ÿÿ\, f\, ÿ\, 2ÿÿ\, p)ÿÿ\, f\, ÿ\, mf Llf\sin ÿf(\ddot{y}_f\, ÿ\, 2\ddot{y}_p)\, f\\
&+ lf\, ÿ\ddot{y}_{pÿf} + lf\, ry(\ddot{y}_p\, ÿ\, nf\ddot{y}_f)\\
&2\, ÿ\, mbl^{ÿÿ^2}\sin ÿp\cos ÿp + mblÿÿ_p\sin ÿp(\ddot{x}_v\cos ÿ + ÿ\ddot{v}\sin ÿ)\, ÿ\, mblÿÿ_p\cos ÿp(\ddot{x}_{ÿv}\sin ÿ + ÿ\ddot{v}\cos ÿ)\\
&ÿ\, Ix\, ÿÿ^2\sin ÿp\cos ÿp + Izzÿÿ^2\sin ÿ\cos ÿ\, ÿ\, mf(L^2{}_{ÿÿ^2}\sin ÿp\cos ÿp\, ÿ\, l\, f^2{}_{ÿÿ^2}\sin ÿfÿp\cos ÿfÿp)\\
&+ mf Lÿÿ_p\sin ÿp(\ddot{x}_v\cos ÿ + ÿ\ddot{v}\sin ÿ)\, ÿ\, mf Lÿÿ\cos ÿp(\ddot{x}_{ÿv}\sin ÿ + ÿ\ddot{v}\cos ÿ)\\
&+ mf lf ÿÿ\sin ÿfÿp(\ddot{x}_{ÿv}\sin ÿ + ÿ\ddot{v}\cos ÿ)\, ÿ\, mf lf ÿÿ\, fÿp\cos ÿfÿp(\ddot{x}_v\cos ÿ + ÿ\ddot{v}\sin ÿ)\\
&ÿ\, mf Llf ÿÿ^2\cos ÿf\, ÿ2p\, ÿ\, If\, xÿÿ^2\sin ÿpÿf\cos ÿpÿf + If\, zÿÿ^2\cos ÿpÿf\sin ÿpÿf\\
&ÿ\, (If\, rx\ ÿ\, If\, rz)ÿÿ^2\sin(ÿp\, ÿ\, nf\, ÿf)\cos(ÿp\, ÿ\, nf\, ÿf)\\
&ÿ\, mblg\sin ÿp\, ÿ\, mf gL\sin ÿp\, ÿ\, mf glf\cos ÿfÿp = 0
\end{aligned}
\tag{2.108}
$$

Next, the Lagrange equation for ÿf is given by equation (2.109) .

$$
\frac{d}{dt}\left(\frac{ÿL}{ÿÿ_f}\right) - \frac{ÿL}{ÿÿf} = nf\, ÿf \tag{2.109}
$$

By calculating each element of equation (2.109) , equation (2.112) can be obtained from equation (2.110) .

$$
\begin{aligned}
\frac{ÿL}{ÿÿ_f} &= mf l^2 ÿÿ\, fÿp\, ÿ\, mf lf\sin ÿfÿp(\ddot{x}_v\cos ÿ + ÿ\ddot{v}\sin ÿ)\, f\\
&\quad ÿ\, mf Llf ÿÿ_p\sin ÿf\, ÿ\, If\, ÿÿÿ\, pÿf\, ÿ\, If\, rynf(ÿÿ\, p\, ÿ\, nf\, ÿÿ\, f)
\end{aligned}
\tag{2.110}
$$

$$
\begin{aligned}
\frac{d}{dt}\left(\frac{ÿL}{ÿÿ_f}\right) &= mf l^2\ddot{y}_{fÿp}\, ÿ\, mf lf\, ÿÿ\, fÿp\cos ÿfÿp(\ddot{x}_v\cos ÿ + ÿ\ddot{v}\sin ÿ)\, f\\
&\quad ÿ\, mf lf\sin ÿfÿp(\ddot{x}_v\cos ÿ\, ÿ\, x\ddot{y}_{vÿÿ}\sin ÿ + \ddot{y}_v\sin ÿ + ÿ\ddot{v}_{ÿÿ}\cos ÿ)\\
&\quad ÿ\, mf Llf(\ddot{y}_p\sin ÿf + ÿÿ\, pÿÿ\, f\cos ÿf)\, ÿ\, If\, ÿ\ddot{y}_{pÿf}\, ÿ\, If\, rynf(\ddot{y}_p\, ÿ\, nf\, \ddot{y}_f)
\end{aligned}
\tag{2.111}
$$

$$
\begin{aligned}
\frac{ÿL}{ÿÿf} &= ÿ\, mf l\, f\, ÿÿf^{2}{}_{ÿÿ^2}\cos ÿfÿp\sin ÿfÿp\, ÿ\, mf lf\, ÿÿ\sin ÿfÿp(\ddot{x}_{ÿv}\sin ÿ + ÿ\ddot{v}\cos ÿ)\\
&\quad ÿ\, mf lf\, ÿÿ\, fÿp\cos ÿfÿp(\ddot{x}_v\cos ÿ + ÿ\ddot{v}\sin ÿ)\, ÿ\, mf Llf(ÿÿ^2\sin ÿp\sin ÿfÿp + ÿÿ\, pÿÿ\, fÿp\cos ÿf)\\
&\quad ÿ\, (If\, x\ ÿ\, If\, z)ÿÿ^2\sin ÿpÿf\cos ÿpÿf\, ÿ\, (If\, rx\ ÿ\, If\, rz)ÿÿ^2 nf\sin(ÿp\, ÿ\, nf\, ÿf)\cos(ÿp\, ÿ\, nf\, ÿf)\\
&\quad ÿ\, mf lf\, g\cos ÿfÿp
\end{aligned}
\tag{2.112}
$$

From equations (2.111) and (2.112) , the equation of motion for ÿf is shown in equation (2.113) .

$$
\begin{aligned}
& mf\, l^2{}_{ÿ^{¨}}\, fÿp\, ÿ\, mf\, lf\, ÿÿ\, fÿp \cos ÿfÿp(\, ÿxv \cos ÿ + yÿv \sin ÿ)\, f \\
& ÿ\, mf\, lf \sin ÿfÿp(\, ¨xv \cos ÿ\, ÿ\, xÿvÿÿ \sin ÿ + y¨v \sin ÿ + yÿvÿÿ \cos ÿ) \\
& ÿ\, mf\, Llf(ÿ¨\, p \sin ÿf + ÿÿ\, pÿÿ\, f \cos ÿf)\, ÿ\, lf\, yÿ¨\, pÿf\, ÿ\, lf\, rynf(ÿ¨\, p\, ÿ\, nf\, ÿ¨\, f) \\
& + mf\, l\, f^{2}_{ÿÿ}{}^{2} \cos ÿfÿp \sin ÿfÿp + mf\, lf\, ÿÿ \sin ÿfÿp(ÿxÿv \sin ÿ + yÿv \cos ÿ) \\
& + mf\, lf\, ÿÿ\, fÿp \cos ÿfÿp(\, ÿxv \cos ÿ + yÿv \sin ÿ) + mf\, Llf(ÿÿ^{2} \sin p \sin fÿp + ÿÿ\, pÿÿ\, fÿp \cos ÿf) \\
& + (lf\, x\, ÿ\, lf\, z)ÿÿ^{2} \sin ÿpÿf \cos ÿpÿf + (lf\, rx \quad ÿ\, lf\, rz)ÿÿ^{2}\, nf \sin(ÿp\, ÿ\, nf\, ÿf) \cos(ÿp\, ÿ\, nf\, ÿf) \\
& + mf\, lf\, g \cos ÿfÿp = nf\, ÿf
\end{aligned}
\tag{2.113}
$$

Summarizing the above results, the Lagrangian equation of motion is given by equation (2.114) .

$$M(q)¨q + V(q, qÿ) + G(q) = Eÿ \tag{2.114}$$

Each matrix is shown in equations (2.115) to (2.117) .

$$
M(q) = \begin{bmatrix}
ÿ\ m11 & 0 & m13 & 0 & & ÿ\ 0 & m16 & m17 \\
0 & m22 & m23 & 0 & m31 & 0 & m26 & m27 & 0 \\
m32 & m33 & 0 & & & 0 & & 0 & \\
0 & 0 & 0 & m44 & 0 & m46 & 0 & 0 & 0 & m55 \\
0 & 0 & m56 & 0 & & & & & & \\
m61 & m62 & 0 & m64 & m65 & m66 & 0 & 0 & 0 & m76 \\
m71 & m72 & 0 & & m77 & & & & &
\end{bmatrix}
\tag{2.115}
$$

$$V(q, qÿ) = [\ \mathbf{v1}\ v2\ v3\ 0\ 0\ v6\ v7\ ]T \tag{2.116}$$

$$G(q) = [\ \mathbf{0}\ 0\ 0\ 0\ 0\ g6\ g7\ ]T \tag{2.117}$$

The elements of the matrices in equations (2.115) to (2.117) are shown in equations (2.118) to (2.137) .

$$m11 = m22 = 2mw + mb + mf \tag{2.118}$$

$$m13 = m31 = ÿ(mbl + mf L) \sin ÿp \sin ÿ ÿ\, mf\, lf \cos ÿfÿp \sin ÿ \tag{2.119}$$

$$m16 = m61 = (mbl + mf L) \cos ÿp \cos ÿ + mf\, lf \sin ÿfÿp \cos ÿ \tag{2.120}$$

$$m17 = m71 = ÿmf\, lf \sin ÿfÿp \cos ÿ \tag{2.121}$$

$$m23 = m32 = (mbl + mf L) \sin ÿp \cos ÿ + mf\, lf \cos ÿfÿp \cos ÿ \tag{2.122}$$

$$m26 = m62 = (mbl + mf L) \cos ÿp \sin ÿ + mf\, lf \sin ÿfÿp \sin ÿ \tag{2.123}$$

$$m27 = m72 = ÿmf\, lf \sin ÿfÿp \sin ÿ \tag{2.124}$$

$$\begin{aligned} m33 = {} & (2mwb^2 + 2Iwz + 2Irz + Ixx \sin2 ÿp + If\, x \sin2 ÿpÿf + If\, rx \sin2 (ÿp ÿ nf ÿf)) \\ & + (Izz \cos2 ÿp + If\, z \cos2 ÿpÿf + If\, rz \cos2 (ÿp ÿ nf ÿf) + 2mf\, lf\, L \sin 2ÿf) \end{aligned} \tag{2.125}$$

$$m44 = m55 = Iwy + n_w^2 Iry \tag{2.126}$$

$$m46 = m64 = m56 = m65 = Iwy + nwIry \tag{2.127}$$

$$m66 = 2(Iwy + Iry) + mbl^2 + Iyy + mf\, L^2 + 2mf\, Llf \sin ÿf + If\, y + mf\, lf - Ifry_f^2 \tag{2.128}$$

$$m67 = m76 = ÿmf\, l_f^2 ÿ\, mf\, Llf \sin ÿf ÿ\, If\, y ÿ\, nf\, If\, ry \tag{2.129}$$

$$m77 = mf\, l_f^2 + If\, y^2 + n_f\, If\, ry \tag{2.130}$$

$$\begin{aligned} v1 = {} & ÿ\,(mbl + mf L)(ÿÿ_p^2 \sin ÿp \cos ÿ + 2ÿÿ\, pÿÿ \cos ÿp \sin ÿ + ÿÿ^2 \sin ÿp \cos ÿ) \\ & ÿ\, mf\, lf(ÿÿ_{fÿp}^2 \cos ÿfÿp \cos ÿ ÿ\, 2ÿÿ\, fÿpÿÿ \sin ÿfÿp \sin ÿ + ÿÿ^2 \cos ÿfÿp \cos ÿ) \end{aligned} \tag{2.131}$$

$$\begin{aligned} v2 = {} & (mbl + mf L)(ÿÿÿ_p^2 \sin ÿp \sin ÿ + 2ÿÿ\, pÿÿ \cos ÿp \cos ÿ ÿ\, ÿÿ^2 \sin ÿp \sin ÿ) \\ & ÿ\, mf\, lf(ÿÿ_{fÿp}^2 \cos ÿfÿp \sin ÿ + 2ÿÿ\, fÿpÿÿ \sin ÿfÿp \cos ÿ + ÿÿ^2 \cos ÿfÿp \sin ÿ) \end{aligned} \tag{2.132}$$

$$\begin{aligned} v3 = {} & ÿ\,(mblsin ÿp + mf\, L \sin ÿp + mf\, lf \cos ÿfÿp)(\, ÿxvÿÿ \cos ÿ + yÿvÿÿ \sin ÿ) \\ & + (mblÿÿ_p \cos ÿp + mf\, Lÿÿ_p \cos ÿp ÿ\, mf\, lf\, ÿÿ\, fÿp \sin ÿfÿp)(ÿxÿv \sin ÿ + yÿv \cos ÿ) \\ & + (Ixxÿÿ_p \sin 2ÿp + If\, xÿÿ\, pÿf \sin 2ÿpÿf + If\, rx(ÿÿ_p ÿ\, nf\, ÿÿ\, f) \sin 2(ÿp ÿ nf ÿf))ÿÿ \\ & ÿ\, (Izzÿÿ_p \sin 2ÿp + If\, zÿÿ\, pÿf \sin 2ÿpÿf + If\, rz(ÿÿ_p ÿ\, nf\, ÿÿ\, f) \sin 2(ÿp ÿ nf ÿf))ÿÿ \\ & + 4mf\, lf\, Lÿÿÿÿ\, f \cos 2ÿf ÿ\, (mbl + mf L)ÿÿ_p \cos ÿp(ÿxÿv \sin ÿ + yÿv \cos ÿ) \\ & + (mbl + mf L)ÿÿ \sin ÿp(\, ÿxv \cos ÿ + yÿv \sin ÿ) \\ & + mf\, lf\, ÿÿ \cos ÿfÿp(\, ÿxv \cos ÿ + yÿv \sin ÿ) ÿ\, mf\, lf\, ÿÿ\, fÿp \sin ÿfÿp(\, ÿxv \sin ÿ ÿ\, yÿv \cos ÿ) = 0 \end{aligned} \tag{2.133}$$

v6 =(ÿmblÿÿ p sin ÿp ÿ mf Lÿÿ p sin ÿp + mf lf ÿÿ fÿp cos ÿfÿp)(ÿxv cos ÿ + yÿv sin ÿ)

+ (mbl cos ÿp + mf L cos ÿp + mf lf sin ÿfÿp)(ÿxÿvÿÿ sin ÿ + yÿvÿÿ cos ÿ) ÿ mf Llf cos ÿf(ÿÿ f ÿ 2ÿÿ p)ÿÿ f sin ÿp

2 ÿ mbl ÿÿ2 cos ÿp + mblÿÿ p sin ÿp(ÿxv cos ÿ + yÿv sin ÿ) ÿ mblÿÿ p cos ÿp(ÿxÿv sin ÿ + yÿv cos ÿ)

ÿ Ixxÿÿ2 sin ÿp cos ÿp + Izzÿÿ2 sin ÿ cos ÿ ÿ mf(L 2ÿÿ2 sin ÿp cos ÿp ÿ l f 2ÿÿ2 sin ÿfÿp cos ÿfÿp)

+ mf Lÿÿÿÿp sin ÿp(ÿxv cos ÿ + yÿv sin ÿ) ÿ mf Lÿÿ cos ÿp(ÿxÿv sin ÿ + yÿv cos ÿ)

+ mf lf ÿÿ sin ÿfÿp(ÿxÿv sin ÿ + yÿv cos ÿ) ÿ mf lf ÿÿ fÿp cos ÿfÿp(ÿxv cos ÿ + yÿv sin ÿ)

ÿ mf Llf ÿÿ 2 cos ÿf ÿ lf xÿÿ 2 sin ÿpÿf cos ÿpÿf + lf zÿÿ 2 cos ÿpÿf sin ÿpÿf

ÿ (If rx ÿ lf rz)ÿÿ2 sin(ÿp ÿ nf ÿf) cos(ÿp ÿ nf ÿf) (2.134)

v7 = ÿ mf lf ÿÿ fÿp cos ÿfÿp(ÿxv cos ÿ + yÿv sin ÿ)

ÿ mf lf sin ÿfÿp(ÿxÿvÿÿ sin ÿ + yÿvÿÿ cos ÿ)

ÿ mf Llf ÿÿ pÿÿ f cos ÿf

+ mf l 2fÿÿ2 cos ÿfÿp sin ÿfÿp + mf lf ÿÿ sin ÿfÿp(ÿxÿv sin ÿ + yÿv cos ÿ)

+ mf lf ÿÿfÿp cos ÿfÿp(ÿxv cos ÿ + yÿv sin ÿ) + mf Llf(ÿÿ 2 sinp sinfÿp +ÿÿ pÿÿ fÿp cos ÿf)

+ (If x ÿ lf z)ÿÿ2 sin ÿpÿf cos ÿpÿf + (If rx ÿ lf rz)ÿÿ2 nf sin(ÿp ÿ nf ÿf) cos(ÿp ÿ nf ÿf) (2.135)

g6 = ÿ mblg sin ÿp ÿ mf Lg sin ÿp ÿ mf glf cos ÿfÿp (2.136)

g7 =mf lf g cos ÿfÿp (2.137)

2.2.3 Equation of motion considering constraint conditions

In this section, we consider the constraint conditions and the equation of motion derived in the previous section. By combining equations (2.31), (2.34), and (2.35) related to the velocity constraint conditions , we obtain equation (2.138) using the coefficient matrix A(q) , where A(q) is equation (2.139) .

$$A(q)\,\ddot{q} = 0 \tag{2.138}$$

$$A(q) = \begin{bmatrix} \ddot{y} \sin ÿ \; ÿ \cos ÿ & 0 & 0 & 0 & 0 \\ \cos ÿ \; \sin ÿ & b\,ÿR & 0 & ÿR & 0 \\ \cos ÿ \; \sin ÿ \; ÿb & 0 & ÿR & ÿR & 0 \end{bmatrix} \tag{2.139}$$

When the constraints of equation (2.138) are met, the equation of motion is expressed as equation (2.140) using the Lagrange multiplier ÿ .

This results in:

$$M(q)\ddot{q} + V(q, q\dot{\varphi}) + G(q) + \mathbf{A}^T(\varphi q)\lambda = E\tau \tag{2.140}$$

The new generalized coordinate τ is defined as shown in equation (2.141) . The relationship in equation (2.142) holds between the previous generalized coordinate q and the new generalized coordinate τ . However, the matrix S(q) is expressed by equation (2.143) .

$$\tau = [\, v \quad \dot{\varphi}_p \quad \dot{\varphi}_f \,]^T \tag{2.141}$$

$$q\dot{\varphi} = S(q)\tau \tag{2.142}$$

$$S(q) = \begin{bmatrix} \frac{1}{2} & \frac{b}{R} & 0 \\ \frac{1}{2} & -\frac{b}{R} & 0 \\ 0 & 0 & 1 \\ 0 & 0 & 1 \end{bmatrix} \tag{2.143}$$

The relationship between A(q) and S(q) is given by equation (2.144) .

$$A(q)S(q) = S(q)^T A(q) = 0 \tag{2.144}$$

By differentiating both sides of equation (2.142) , equation (2.145) holds.

$$\ddot{q} = S(q)\dot{\tau} + S\dot{\varphi}(q)\tau \tag{2.145}$$

By multiplying equation (2.140) by ST (q) from the left and using the results of equations (2.144) and (2.145) , we obtain equation (2.146) , in which the generalized coordinates are replaced with the newly defined ones .

$$S^T(q)M(q)\,(S(q)\dot{\tau} + S\dot{\varphi}(q)\tau) + S^T(q)V(q, q\dot{\varphi}) + S^T(q)G(q) = S^T(q)E \tag{2.146}$$

In equation (2.146) , the constraints are taken into account by using the newly defined matrices $\bar{M}$,$\bar{H}$,$\bar{V}$,$\bar{G}$,and $\bar{E}$.

The equation of motion for the two-wheeled mobile transport robot is given by equation (2.147) .

$$\bar{M}(q)\dot{\tau} + \bar{H}(q, q\dot{\varphi})\tau + \bar{V}(q, q\dot{\varphi}) + \bar{G}(q) = E\bar{\tau} \tag{2.147}$$

where each matrix is from equation (2.148) to equation (2.152) .

$$\bar{M}(q) = S^T(q)M(q)S(q)$$

$$= \begin{bmatrix} \bar{m}_{11} & 0 \\ 0 & \begin{matrix} \bar{m}_{33} & \bar{m}_{34} \\ \bar{m}_{43} & \bar{m}_{44} \end{matrix} \end{bmatrix} \tag{2.148}$$

$$\bar{H}(q) = S^T(q)M(q)S\dot{q}(q)$$

$$= \begin{bmatrix} 0 & 0 \\ 0 & \begin{matrix} 0 & 0 & 0 \\ 0 & 0 & 0 \\ 0 & 0 & 0 \end{matrix} \end{bmatrix} \tag{2.149}$$

$$\bar{V}(q,q\dot{q}) = S^T(q)V(q,q\dot{q})$$

$$= [\,\bar{v}_1 \; \bar{v}_2 \; \bar{v}_3 \; \bar{v}_4\,]^T \tag{2.150}$$

$$\bar{G}(q) = S^T(q)G(q)$$

$$= \begin{bmatrix} 0 \\ 0 \\ -(m_b l_g \sin\theta_p + m_f L_g \sin\theta_p + m_f l_f \cos\theta_f\theta_p + m_f l_f g \cos\theta_f\theta_p) \end{bmatrix} \tag{2.151}$$

$$\bar{E}(q) = S^T(q)E(q)$$

$$= \begin{bmatrix} \frac{n_w}{R} & \frac{n_w}{R} & \dot{\theta}_0 \\ \frac{b n_w}{R} & -\frac{b n_w}{R} & 0 \\ -n_w & -n_w & 0 \\ 0 & 0 & n_f \end{bmatrix} \tag{2.152}$$

The elements of equations (2.148) to (2.152) are shown in equations (2.153) to (2.163) .

$$m^{-}11 = 2mw + mb + mf + \frac{2}{R2}(Iwy + nw\ Iry)^2 \tag{2.153}$$

$$L)\cos ÿp + mf\ lf \sin ÿfÿp + (nw ÿ\ nm^{-}13 = m^{-}31 \qquad \overline{R}^{2}{}_{2} = (mbl + mf \qquad w\ )Iry \tag{2.154}$$

$$m^{-}14 = m^{-}41 = ÿmf\ lf \sin ÿfÿp \tag{2.155}$$

$$m^{-}22 = (2mwb^{2} + 2Iwz + 2Irz + Ixx \sin 2 ÿp + If\ x \sin 2 ÿpÿf + If\ rx \sin 2 (ÿp ÿ\ nf\ ÿf))$$
$$+ (Izz \cos 2 ÿp + If\ z \cos 2 ÿpÿf + If\ rz \cos 2 (ÿp ÿ\ nf\ ÿf) + 2mf\ lf\ L \sin 2ÿf)$$
$$+ \frac{2\ 2b}{R2}(Iwy + n^{2}_{w}\ Iry) \tag{2.156}$$

$$m^{-}33 = mbl^{2} + mf\ l^{2} + mf\ L\ f^{2} + 2mf\ Llf \sin ÿf + Iyy + If\ y \qquad + Ifry \quad + 2(nw ÿ\ 1)2\ Iry \tag{2.157}$$

$$m^{-}34 = m43 = ÿmf\ l^{2}_{f} ÿ\ mf\ Llf \sin ÿf ÿ\ If\ y ÿ\ nf\ If\ ry \tag{2.158}$$

$$m^{-}44 = mf\ l^{2}_{f} + If\ y^{2} + n_{f\ If\ ry} \tag{2.159}$$

$$v^{-}1 = ÿ\ (mbl + mf\ L)(ÿÿ^{2}_{p} \sin ÿp + ÿÿ^{2} \sin ÿp)$$
$$ÿ\ mf\ lf(ÿÿ^{2}_{fÿp} \quad cosÿf\ ÿp + ÿÿ^{2} \cos ÿfÿp) \tag{2.160}$$

$$v^{-}2 = ÿ\ (mblsin ÿp + mf\ L \sin ÿp + mf\ lf \cos ÿfÿp)(ÿxvÿÿ \cos ÿ + yÿvÿÿ \sin ÿ)$$
$$+ (mblÿÿ_{p} \cos ÿp + mf\ Lÿÿ_{p} \cos ÿp ÿ\ mf\ lf\ ÿÿ\ fÿp \sin ÿfÿp)(ÿxÿv \sin ÿ + yÿv \cos ÿ)$$
$$+ (Ixxÿÿ_{p} \sin 2ÿp + If\ xÿÿ\ pÿf \sin 2ÿpÿf + If\ rx(ÿÿ_{p}\ ÿ\ nf\ ÿÿ\ f) \sin 2(ÿp ÿ\ nf\ ÿf))ÿÿ$$
$$ÿ\ (Izzÿÿ_{p} \sin 2ÿp + If\ zÿÿ\ pÿf \sin 2ÿpÿf + If\ rz(ÿÿ_{p}\ ÿ\ nf\ ÿÿ\ f) \sin 2(ÿp ÿ\ nf\ ÿf))ÿÿ$$
$$+ 4mf\ lf\ Lÿÿÿÿ\ f \cos 2ÿf ÿ\ (mbl + mf\ L)ÿÿ_{p} \cos ÿp(ÿxÿv \sin ÿ + yÿv \cos ÿ)$$
$$+ (mbl + mf\ L)ÿÿ \sin ÿp(\ ÿxv \cos ÿ + yÿv \sin ÿ)$$
$$+ mf\ lf\ ÿÿ \cos ÿfÿp(\ ÿxv \cos ÿ + yÿv \sin ÿ)\ ÿ\ mf\ lf\ ÿÿ\ fÿp \sin ÿfÿp(\ ÿxv \sin ÿ\ ÿ\ yÿv \cos ÿ) = 0 \tag{2.161}$$

$$\bar{v}3=(\ddot{y}mbl\ddot{y}\ddot{y}\ \ p\ \sin\ddot{y}p\ \ddot{y}\ mf\ L\ddot{y}\ddot{y}\ \ p\ \sin\ddot{y}p + mf\ lf\ \ddot{y}\ddot{y}\ f\ddot{y}pcos\ \ddot{y}f\ddot{y}p)(\ \ddot{y}xv\cos\ddot{y} + y\ddot{y}v\sin\ddot{y})$$

$$+ (mbl\cos\ddot{y}p + mf\ L\cos\ddot{y}p + mf\ lf\sin\ddot{y}f\ddot{y}p)(\ddot{y}x\ddot{y}v\ddot{y}\ddot{y}\sin\ddot{y} + y\ddot{y}v\ddot{y}\ddot{y}\cos\ddot{y})\ \ddot{y}\ mf\ Llf\cos\ddot{y}f(\ddot{y}\ddot{y}\ f\ \ddot{y}\ 2\ddot{y}\ddot{y}\ p)\ddot{y}\ddot{y}\ f$$

$$\ddot{y}\ mbl\ \ {}^{2}_{\ddot{y}\ddot{y}}{}^{2}\sin\ddot{y}p\cos\ddot{y}p + mbl\ddot{y}\ddot{y}\ \ p\ \sin\ddot{y}p(\ \ddot{y}xv\cos\ddot{y} + y\ddot{y}v\sin\ddot{y})\ \ddot{y}\ mbl\ddot{y}\ddot{y}\ \ p\ \cos\ddot{y}p(\ddot{y}x\ddot{y}v\sin\ddot{y} + y\ddot{y}v\cos\ddot{y})$$

$$\ddot{y}\ lx\ x\ddot{y}\ddot{y}\ \ {}^{2}\sin\ddot{y}p\cos\ddot{y}p + Izz\ddot{y}\ddot{y}\ \ {}^{2}\sin\ddot{y}\cos\ddot{y}\ \ddot{y}\ mf(L\ \ {}^{2}_{\ddot{y}\ddot{y}}{}^{2}\sin\ddot{y}p\cos\ddot{y}p\ \ddot{y}\ l\ \ {}^{2}_{f}{}^{\ddot{y}\ddot{y}}{}^{2}\sin\ddot{y}f\ddot{y}p\cos\ddot{y}f\ddot{y}p)$$

$$+ mf\ L\ddot{y}\ddot{y}\ \ p\ \sin\ddot{y}p(\ \ddot{y}xv\cos\ddot{y} + y\ddot{y}v\sin\ddot{y})\ \ddot{y}\ mf\ L\ddot{y}\ddot{y}\cos\ddot{y}p(\ddot{y}x\ddot{y}v\sin\ddot{y} + y\ddot{y}v\cos\ddot{y})$$

$$+ mf\ lf\ \ddot{y}\ddot{y}\sin\ddot{y}f\ddot{y}p(\ddot{y}x\ddot{y}v\sin\ddot{y} + y\ddot{y}v\cos\ddot{y})\ \ddot{y}\ mf\ lf\ \ddot{y}\ddot{y}\ f\ddot{y}p\cos\ddot{y}f\ddot{y}p(\ \ddot{y}xv\cos\ddot{y} + y\ddot{y}v\sin\ddot{y})$$

$$\ddot{y}\ mf\ Llf\ \ddot{y}\ddot{y}\ \ {}^{2}\cos\ddot{y}f\ \ddot{y}\ lf\ x\ddot{y}\ddot{y}\ \ {}^{2}\sin\ddot{y}p\ddot{y}f\cos\ddot{y}p\ddot{y}f + lf\ z\ddot{y}\ddot{y}\ \ {}^{2}\cos\ddot{y}p\ddot{y}f\sin\ddot{y}p\ddot{y}f$$

$$\ddot{y}\ (lf\ rx\ \ \ddot{y}\ lf\ rz)\ddot{y}\ddot{y}\ \ {}^{2}\sin(\ddot{y}p\ \ddot{y}\ nf\ \ddot{y}f)\cos(\ddot{y}p\ \ddot{y}\ nf\ \ddot{y}f) \tag{2.162}$$

$$\bar{v}4=\ \ddot{y}\ mf\ lf\ \ddot{y}\ddot{y}\ f\ddot{y}p\cos\ddot{y}f\ddot{y}p(\ \ddot{y}xv\cos\ddot{y} + y\ddot{y}v\sin\ddot{y})$$

$$\ddot{y}\ mf\ lf\sin\ddot{y}f\ddot{y}p(\ddot{y}x\ddot{y}v\ddot{y}\ddot{y}\sin\ddot{y} + y\ddot{y}v\ddot{y}\ddot{y}\cos\ddot{y})$$

$$\ddot{y}\ mf\ Llf\ \ddot{y}\ddot{y}\ p\ddot{y}\ddot{y}\ f\cos\ddot{y}f$$

$$+ mf\ l\ \ {}^{2}_{f}{}^{\ddot{y}\ddot{y}}{}^{2}\cos\ddot{y}f\ddot{y}p\sin\ddot{y}f\ddot{y}p + mf\ lf\ \ddot{y}\ddot{y}\sin\ddot{y}f\ddot{y}p(\ddot{y}x\ddot{y}v\sin\ddot{y} + y\ddot{y}v\cos\ddot{y})$$

$$+ mf\ lf\ \ddot{y}\ddot{y}\ f\ddot{y}p\cos\ddot{y}f\ddot{y}p(\ \ddot{y}xv\cos\ddot{y} + y\ddot{y}v\sin\ddot{y}) + 2mf\ Llf(\ddot{y}\ddot{y}\ \ {}^{2}\sin p\ \sin f\ddot{y}p + \ddot{y}\ddot{y}\ p\ddot{y}\ddot{y}\ f\ddot{y}p\cos\ddot{y}f)$$

$$+ (lf\ x\ \ \ddot{y}\ lf\ z)\ddot{y}\ddot{y}\ \ {}^{2}\sin\ddot{y}p\ddot{y}f\cos\ddot{y}p\ddot{y}f + (lf\ rx\ \ \ddot{y}\ lf\ rz)\ddot{y}\ddot{y}\ \ {}^{2}nf\sin(\ddot{y}p\ \ddot{y}\ nf\ \ddot{y}f)\cos(\ddot{y}p\ \ddot{y}\ nf\ \ddot{y}f) \tag{2.163}$$

In addition, in this study, we consider the case of moving a two-wheeled mobile robot in the forward and backward directions, so we assume that the robot is XW

Consider that the vehicle travels on an axis. Eliminate the turning component from equation (2.147) and obtain equations (2.165) and (2.166) . Using this relationship, the equations of motion for the wheel rotation angle, pitch angle, and fork angle are rearranged to obtain equation (2.164).

This results in:

$$\bar{M}\ddot{y}\ (q)\ \ddot{y}\ddot{y} + \bar{V}\ddot{y}\ (q, q\ddot{y}) + \bar{G}\ddot{y}\ (q) = \bar{E}\ddot{y}\ddot{y} \tag{2.164}$$

$$xv = R\ddot{y}w \tag{2.165}$$

$$yv = \ddot{y} = 0 \tag{2.166}$$

where each matrix is from equation (2.167) to equation (2.170) .

$$\bar{M}(q) = \begin{bmatrix} \bar{m}_{11} & \bar{m}_{12} & \bar{m}_{13} \\ \bar{m}_{21} & \bar{m}_{22} & \bar{m}_{23} \\ \bar{m}_{31} & \bar{m}_{32} & \bar{m}_{33} \end{bmatrix} \tag{2.167}$$

$$\bar{V}(q, \dot{q}) = S^T(q)V(q, \dot{q}) = [\bar{v}_1 \quad \bar{v}_2 \quad \bar{v}_3]^T \tag{2.168}$$

$$\bar{G}(q) = S^T(q)G(q) = \begin{bmatrix} 0 \\ -mblg\sin\theta_p - mfLg\sin\theta_p - mfglf\cos\theta_f\theta_p \\ -mflfg\cos\theta_f\theta_p \end{bmatrix} \tag{2.169}$$

$$\bar{E}(q) = S^T(q)E(q) = \begin{bmatrix} nw & -nw & 0 \\ -nw & nw & 0 \\ 0 & 0 & nf \end{bmatrix} \tag{2.170}$$

Each element of equations (2.167) to (2.170) is shown in equations (2.171) to (2.171) .

$$\bar{m}_{11} = (2mw + mb + mf)R^2 + 2(Iwy + n^2 Iry) \tag{2.171}$$

$$\bar{m}_{21} = \bar{m}_{12} = (mbl + mfL)R\cos\theta_p + mflfR\sin\theta_f\theta_p + 2(nw - n)^2 Iry \tag{2.172}$$

$$\bar{m}_{31} = \bar{m}_{13} = -mflfR\sin\theta_f\theta_p \tag{2.173}$$

$$\bar{m}_{22} = mbl^2 + mfl_f^2 + mfL^2 + Iyy + 2mfLlf\sin\theta_f + Ify + Ifry + 2(nw - 1)^2 Iry \tag{2.174}$$

$$\bar{m}_{32} = \bar{m}_{23} = -mfl_f^2 - mflf\sin\theta_f - Ify - nfIfry \tag{2.175}$$

$$\bar{m}_{33} = mfl_f^2 + Ify + n^2 Ifry \tag{2.176}$$

$$\bar{v}_1 = -(mbl + mfL)R\dot{\theta}_p^2 \sin\theta_p - mfR\dot{\theta}_f^2 \cos\theta_f\theta_p \tag{2.177}$$

$$\bar{v}_2 = -mflf\cos\theta_f(\dot{\theta}_f - 2\dot{\theta}_p)\dot{\theta}_f \tag{2.178}$$

$$\bar{v}_3 = -mflf\dot{\theta}_p^2 \cos\theta_f \tag{2.179}$$

Chapter **3**

Control System Design

In this chapter, we explain the control system design of the two-wheeled mobile transport robot. First, we design the Unified Pitch Angle Disturbance Observer (SPADO) that is applied to the body part , and the Repulsive Compliance Control (RCC) We discuss the compensation of the center of gravity deviation by the tracking control and the attitude stabilization control based on the Lyapunov stability theorem. Next, we will explain the disturbance observer and reaction torque estimation observer applied to the fork part. First, we explain the proposed method, compliance control, and finally We will now explain the fork angle command value generator that uses these.

3.1 Unified Pitch Angle Disturbance Observer **(SPADO)**

In this chapter, we propose a method to estimate the pitch angle and disturbance acting on the wheel angle of a two-wheeled mobile transport robot. The equations of motion for the wheel rotation angle ÿw and pitch angle ÿp are obtained by rearranging equation (2.164) as equations (3.1) and (3.2) , respectively.

$$m_{\ddot{y}\,11\ddot{y}}\ddot{w}_{es} + m^{-}_{\ddot{y}\,12\ddot{y}}\ddot{p}_{es} + m^{-}_{\ddot{y}\,13\ddot{y}}\ddot{f}_{res} + v^{-}{}'_{1} = n_{w\ddot{y}}\ddot{w}^{ref} \ddot{y}\, T_{lw} \tag{3.1}$$

$$m_{\ddot{y}\,21\ddot{y}}\ddot{w}_{es} + m^{-}_{\ddot{y}\,22\ddot{y}}\ddot{p}_{es} + m^{-}_{\ddot{y}\,23\ddot{y}}\ddot{f}_{res} + v^{-}{}' + g_2 = \ddot{y}n_{w\ddot{y}2}\ddot{w}^{ref} \ddot{y}\, T_{lp} \tag{3.2}$$

The rotor torques ÿr and ÿl of the left and right wheels are expressed together as in equation (3.3) . Furthermore, g2 is related to the pitch angle.

The gravity term that has an influence is shown in equation (3.4) . Tlw and Tlp represent disturbance terms including external forces and friction.

$$\ddot{y}w = \ddot{y}r + \ddot{y}l \tag{3.3}$$

$$g2 = \ddot{y}mblg \sin \ddot{y}p \ddot{y} mf Lg \sin \ddot{y}p \ddot{y} mf glf \cos \ddot{y}f\ddot{y}p \tag{3.4}$$

where ÿres and ÿref represent the response value and reference value, respectively.

Next, we consider nominalizing the inertia term. To remove the nonlinear term, we use the nominal matrix of the inertia term in equation (3.5): That's it.

$$M\bar{\ddot{y}}_{n} = \begin{matrix} \ddot{y} m'_{n11} & m'_{n12} & m'_{n13} \ddot{y} \\ m'_{n21} & m'_{n22} & m'_{n23} \\ \bar{m}'_{n31} & m'_{n32} & m'_{n33} \bar{} \end{matrix} \tag{3.5}$$

The elements of equation (3.5) are shown in equations (3.6) to (3.11) .

$$m'_{n11} = (2mw + mb + mf)R^2 + 2(Iwy + nwIry^2) \tag{3.6}$$

$$\ddot{y}\ddot{y} m = mn12n21 = (mbl + mf L)R + 2(nw \ddot{y} n)^2 Iry \tag{3.7}$$

$$m'_{n13} \quad \ddot{y} = m\, n31 = 0 \tag{3.8}$$

$$\ddot{y} m_{n22}\, 2 = mbl^2 + mf l_f^2 + mf L^2 + Iyy + If y + Ifry + 2(nw \ddot{y} 1)2 Iry \tag{3.9}$$

$$m'_{n23} = m'_{n32} = \ddot{y}mf l f^2 \ddot{y} If y \ddot{y} nf If ry \tag{3.10}$$

$$m'_{n33} = mf l^2 + If yf^2 + n f If ry \tag{3.11}$$

Using the nominal value defined in equation (3.5) , equations (3.1) and (3.2) can be rewritten as equations (3.12) and (3.13) .

However, the ÿ ÿ on the right-hand side of equations (3.12) and (3.13) is dis_{w} dis , ÿ p is the external disturbance term, internal interference force, gravity term and

The total disturbance, which includes the inertial fluctuation and the linear fluctuation, is expressed by equations (3.14) and (3.15), respectively.

$$m'_{n11}\ddot{y}_{wres} \quad ref\ dis\ \ddot{y}\ \ddot{y}\tilde{} = nw\ddot{y}_{w} \tag{3.12}$$

$$m_{\ddot{y}\, n21\ddot{y}_{wres}} + m_{\ddot{y}\, n22\ddot{y}_{pres}} \quad ref\ dis\ \ddot{y}\ \ddot{y}\tilde{} = \ddot{y}nw\ddot{y} \tag{3.13}$$

$$\ddot{y}\tilde{} = m\bar{} \quad \ddot{y}\, 12\ddot{y}_{pres} + m\bar{}_{f} \ddot{y}\, 13\ddot{y}_{res} + (\bar{m}' \quad \ddot{y}\, m\, 11 + v\bar{}'_{1} + Tlw \tag{3.14}$$

$$\ddot{y}\tilde{} = m\bar{}_{p} \quad \ddot{y}\, 23\ddot{y}_{f} res + (\bar{m}' \quad \ddot{y}\, m\, 21 \ddot{y}\, n21)\ddot{y}_{w} res + (\bar{m}' \quad \ddot{y}\, m\, 22 \ddot{y}\, n22)\ddot{y}_{p} res + v\bar{}'_{2} + g\bar{}'_{2} + Tlp \tag{3.15}$$

By eliminating ÿ¨res from equations (3.12) and (3.13) , we obtain equation (3.16) . dis_{s} is ÿ ÿ dis_{w} and ÿ ˜ dis_{p} of

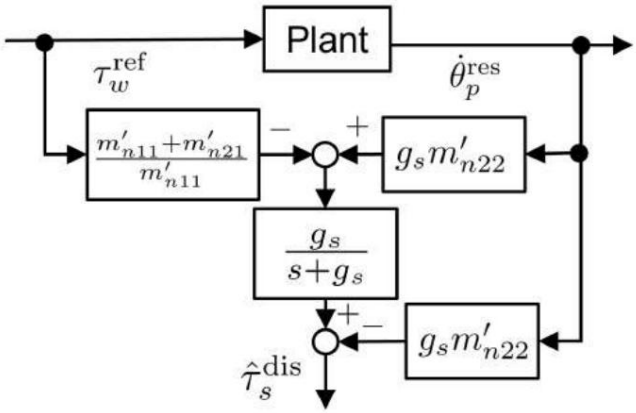

Fig. 3-1: Block diagram of the integrated pitch angle disturbance observer (SPADO)

This is summarized by equation (3.17) and is called the integrated pitch angle disturbance.

$$m_{\ddot{y}\,n22\ddot{y}\,\ddot{p}es} + \frac{\ddot{y}\,\ddot{y}\,m + m\,re\,f\,n21}{m\ddot{y}_{n11}} \quad w \quad s \tag{3.16}$$

$$\ddot{y}\,p_s \quad \text{dis dis}\,\ddot{y}\,\ddot{y} = \ddot{y} \quad \frac{m_{n21\,dis\,\ddot{y}}}{m\ddot{y}_{n11}} \quad s \tag{3.17}$$

In order to suppress the amplification of high-frequency noise due to differentiation, a pseudo-differential method using a first-order low-pass filter is used. The estimated integrated pitch angle disturbance value $\ddot{y}_s^{dis}$ is calculated using equation (3.18) , where s is the Laplace operator and gs is This is the cutoff frequency of the low-pass filter.

$$\ddot{y}_s^{dis} = \frac{gs}{s + gs}\,\ddot{y}_s^{dis} \tag{3.18}$$

By rearranging equation (3.18) using equation (3.16) , the estimated integrated pitch angle disturbance is given by equation (3.19) .

$$\ddot{y}_s^{dis} = \frac{gs}{s + gs\,(\,m} \quad \frac{n21 \quad + m_{n11\,ref\,nw\ddot{y}\,\ddot{y}\,gsm}}{m'_{n11}} \quad w \quad \ddot{y}\,n22\ddot{y}\ddot{y}\,res \quad p\,)\,\ddot{y}\,gsm \quad \ddot{y}\,n22\ddot{y}\ddot{p}es \tag{3.19}$$

Fig. 3-1 shows the block diagram of the integrated pitch angle disturbance observer (SPADO) .

3.2 Repulsive Compliance Control **(RCC)**

In this section, we will describe the generation of pitch angle command values for compensating for the deviation in the center of gravity position using repulsive compliance control (RCC) . Compliance control has the characteristics of both position control and force control. The control follows the reaction force by determining the position command value of the position control according to the force response value. This can be achieved.

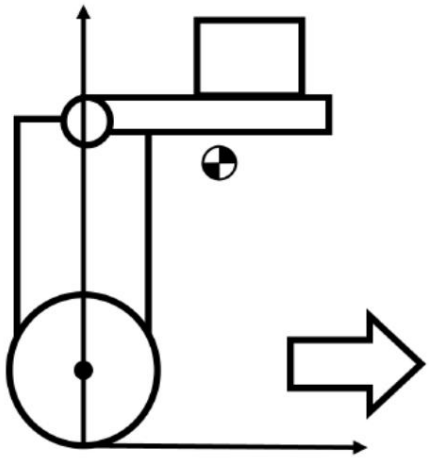

Fig. 3-2: Without RCC

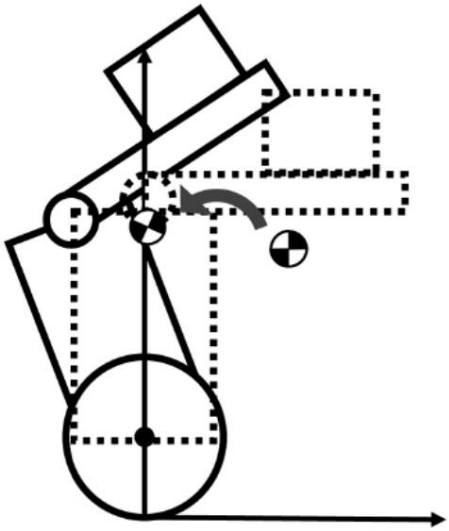

Fig. 3-3: When using RCC

On the other hand, RCC has the property of countering the reaction force by generating a command value in the opposite direction to the force response.

Fig.3-2 and Fig.3-3 show the state in which the transported object is placed on the fork. Fig.3-2 shows the RCC

When the RCC is not used, Fig. 3-3 shows the case where it is used. When a load is placed on the system, the center of gravity of the system changes.

By doing so, disturbances are generated in the pitch angle direction, causing the robot to constantly accelerate.

By doing so, the pitch angle converges to an angle that compensates for the deviation in the center of gravity position, thereby suppressing the

acceleration of the robot caused by the deviation in the center of gravity position. The impedance model in RCC is shown in equation (3.20) .

$$Mrcc\ddot{y}_{PC}^{cmd} + Drcc\dot{y}\dot{y}_{PC}^{cmd} + Krcc\ddot{y}_{PC}^{cmd} = \ddot{y}Arcc\hat{y}f^{ext} \quad (3.20)$$

where Mrcc, Drcc, and Krcc are the virtual inertia, viscosity, and stiffness coefficients, respectively. Arcc is the assist gain of the external force.

The input is the value $\ddot{y}\hat{f}^{ext}$ Use.

By inputting the external force acting on the fork estimated by RTOB into the virtual model, the pitch angle and angular velocity

The command values for the angular acceleration and the stabilization control described in Section 3.4 are generated based on the command values generated by (3.20) .

By using this, the pitch angle moves to follow the command value, compensating for the deviation of the center of gravity position.

The block diagram of the RCC is shown in Figure 1.

Moreover, the transfer function between the input torque and the pitch angle command value is given by equation (3.21) .

$$\frac{cmd\ddot{y}pc}{\ddot{y}\hat{f}^{ext}} = \frac{Arcc}{Mrcc\ s^2 + Drccs + Krcc} \quad (3.21)$$

From equation (3.21) , the transfer function of the RCC is a second-order delay system. Therefore, the characteristics are the natural angular frequency ÿp and the damping ratio

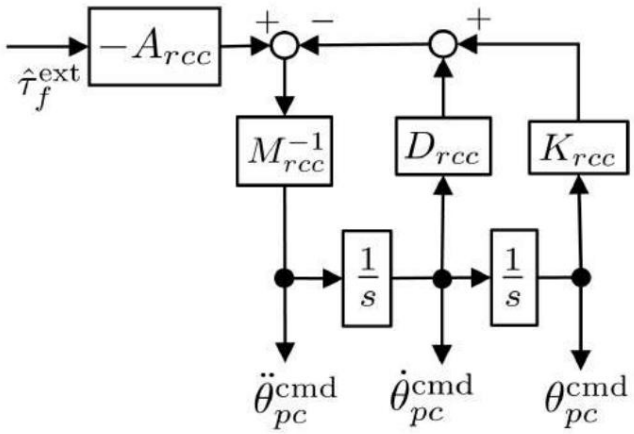

Fig. 3-4: Block diagram of RCC

It is expressed by equation (3.22) using ÿp and the gain Grcc, which is the coefficient that determines the magnitude of the output . Each coefficient can be found from equations (3.23) to (3.25) .

$$\frac{\ddot{y}_{pc}^{\mathrm{cmd}}}{\hat{y}_f^{\mathrm{ext}}} = \frac{\mathrm{Grcc}\ddot{y}_p^2}{2s + 2\ddot{y}p\ddot{y}p\, s + \ddot{y}_p^2} \tag{3.22}$$

$$\ddot{y}p = \ddot{y}\sqrt{\frac{\mathrm{Krcc}}{\mathrm{Mrcc}}} \tag{3.23}$$

$$\mathrm{Drcc}\ddot{y}p = 2\ddot{y}\sqrt{\mathrm{MrccKrcc}} \tag{3.24}$$

$$\mathrm{Grcc} = \frac{\mathrm{Krcc}}{\mathrm{Arcc}} \tag{3.25}$$

The method for determining each parameter is to determine the gain Grcc so that the center of gravity is on the vertical line of the axle when a load of the desired mass is loaded. In addition, the damping ratio ÿp is set to 1 to prevent resonance and speed up the response . Similarly, it is desirable to set the natural angular frequency ÿp large to speed up the response.
It is.

3.3 Pitch angle command value generation

In this section, we explain how to generate the pitch angle command value used in Section 3.4. For a two-wheeled mobile transport robot, it is necessary to ensure posture stability while tracking the target trajectory. For this reason, in this study, a PI controller is used as the wheel angle controller in the outer loop, and a posture stabilization controller based on the Lyapunov stability theorem is used. The controller is a pitch angle controller and is placed in the inner loop to achieve tracking.
This realizes both control and attitude stabilization control.

First, we explain the outer loop that performs tracking control. The two-wheeled mobile transport robot has a center of gravity of the system.

The acceleration and deceleration are achieved by moving the

The inclination of the di becomes the command value for the pitch angle, which is expressed by equation (3.26) .

$$\ddot{y}_{cmd\,pw} = K_{pw}(\dot{y}^{cmd}_{w} - \dot{y}^{res}_{w}) + K_{iw}\int(\dot{y}^{cmd}_{w} - \dot{y}^{res}_{w})dt \tag{3.26}$$

where Kpw and Kiw are the proportional gain and integral gain, respectively. The command value ÿ calculated by equation (3.26) $\ddot{y}^{cmd}_{pw}$

The command value ÿ by RCC obtained in Section 3.2 is $\ddot{y}^{cmd}_{PC}$ The sum of these is the pitch used as input to the attitude stabilization controller.

This becomes the angle command value and is expressed by equation (3.27) .

$$\ddot{y}_{cmd\,p} = \ddot{y}_{pw} + \ddot{y}_{pc} \tag{3.27}$$

3.4 Attitude stabilization controller based on Lyapunov stability theorem

In this section, we explain the posture stabilization controller based on the Lyapunov stability theorem.

The bot is a system that is unstable in the pitch direction, and in order to maintain the inverted state, posture stabilization is required.

In this study, in order to stabilize the system, the wheel torque reference value, which is the control input, is determined based on the Lyapunov stability theorem.

The candidate Lyapunov function V is set as shown in equation (3.28) .

$$V = \frac{1}{2}K_1(\dot{y}^{cmd}_{p} - \dot{y}_{p})^2 + \frac{1}{2}K_2(\dot{y}^{cmd}_{p} - \dot{y}_{p})^2 \tag{3.28}$$

where K1 and K2 are positive gains. The first-order time derivative of equation (3.28) is given by equation (3.29) .

$$\begin{aligned}\dot{V}_{\ddot{y}} &= K_1(\dot{y}^{cmd}_{p} - \dot{y}_{p})(\ddot{y}^{cmd}_{p} - \ddot{y}_{p}) + K_2(\dot{y}^{cmd}_{p} - \dot{y}_{p})(\ddot{y}^{cmd}_{p} - \ddot{y}_{p}) \\ &= (\ddot{y}^{cmd}_{p} - \ddot{y}_{p})\{K_1(\dot{y}^{cmd}_{p} - \dot{y}_{p}) + K_2(\ddot{y}^{cmd}_{p} - \ddot{y}_{p})\}\end{aligned} \tag{3.29}$$

Now, rearranging equation (3.16) with respect to $\ddot{y}^{res}_{p}$ and substituting it into equation (3.29) , we obtain equation (3.30) .

$$\dot{V}_{\ddot{y}} = (\ddot{y}^{cmd}_{p} - \ddot{y}_{p})\left[K_1(\dot{y}^{cmd}_{p} - \dot{y}_{p}) + K_2\left\{\ddot{y}^{cmd}_{p} + \frac{1}{m'_{n22}}\left(\frac{nw(m'_{n21} + m'_{n11})}{m'_{n11}}\dot{y}^{ref} + \dot{y} - \tilde{dis}\right)\right\}\right] \tag{3.30}$$

When equation (3.30) takes the form of equation (3.31) , V is semi-indeterminate and $\dot{V}_{\ddot{y}}$ is zero only at the equilibrium point .

The stability of the system can be guaranteed by the law of eigenvalues. However, K3 is a positive gain .

$$\dot{V}_{\ddot{y}} = -K_3(\ddot{y}^{cmd}_{p} - \ddot{y}_{p})^2 \tag{3.31}$$

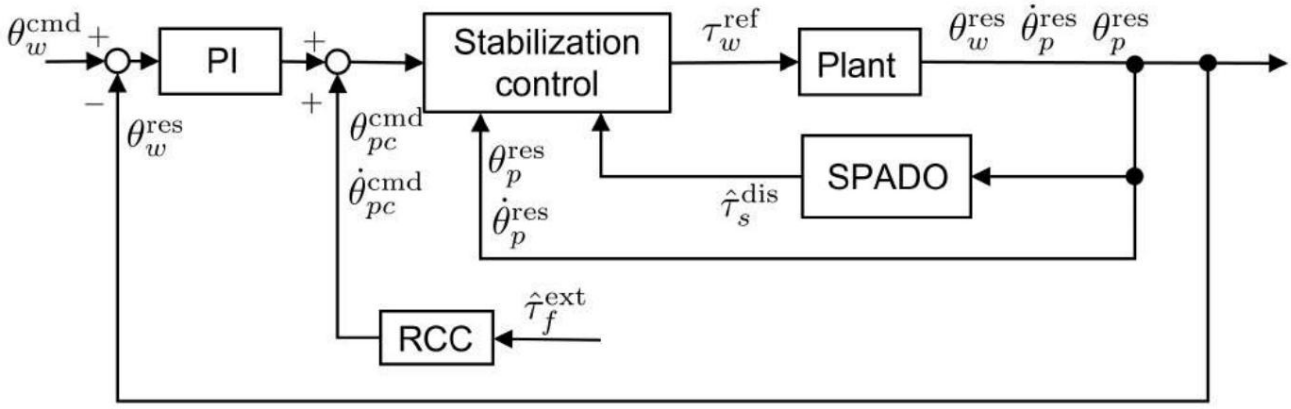

Fig. 3-5: Block diagram of the entire control system for the body

By comparing equation (3.30) and equation (3.31) , equation (3.32) can be obtained.

$$[\,K1(\ddot{y}_p^{cmd} - \ddot{y}_p^{res}) + K2\{\ddot{y}_p^{cmd} - \dot{y}_p^{res}\}] + \frac{1}{m\ddot{y}_{n22}}\left(\frac{nw(m'_{\ddot{y}+m\,n21}\,n11)}{m\ddot{y}_{n11}}\ddot{y}_w^{ref} + \ddot{y}_s^{dis}\right)\} = \ddot{y}K3(\ddot{y}_p^{cmd} - 2\dot{y}_p^{res}\dot{y}_p^{res}) \quad (3.32)$$

Wheel torque reference value $\ddot{y}_w^{ref}$ By changing the equation to (3.33), equation (3.32) is satisfied and stability is guaranteed.

$$\ddot{y}_w^{cmd} = \frac{\ddot{y}\,m'_{n11}m'_{n22} + }{nw(m\ddot{y}_{n21}\ m\ddot{y}\,n11)}\{K2(\ddot{y}_p^{cmd} - \ddot{y}_p^{res}) + \frac{K3}{K2}(\ddot{y}_p^{cmd} - \ddot{y}_p^{res}) + \ddot{y}_p^{cmd}\} + \frac{m'_{n11}}{nw(m\ddot{y}_{n21} + m'\,n11)}\ddot{y}_s^{dis} \quad (3.33)$$

Integrated pitch angle disturbance $\ddot{y}_s^{dis}$ can be accurately estimated, and $\ddot{y}_s^{dis}$ and $\ddot{y}_s^{dis}$ If equal, the estimate is made by (3.19).

The Using the control input $\ddot{y}_w^{ref}$ By changing the equation to (3.34) , $\ddot{y}_p$ and $\dot{y}_p$ can converge to the command value.

Guaranteed.

$$\ddot{y}_w^{ref} = \frac{\ddot{y}\,m'_{n11}m'_{n22}}{nw(m\ddot{y}_{n21} + m\ddot{y}\,n11)}\{Kpp(\ddot{y}_p^{cmd} - \ddot{y}_p^{res}) + Kd_p(\dot{y}_p^{cmd} - \dot{y}_p^{res}) + \ddot{y}_p^{cmd}\} + \frac{m'_{n11}}{nw(m\ddot{y}_{n21} + m'\,n11)}\ddot{y}_s^{dis} \quad (3.34)$$

where Kpp and Kd p are obtained by substituting K1, K2, and K3 from equation (3.33) into equations (3.35) and (3.36) , respectively, denote the proportional gain and differential gain, respectively.

$$Kpp = \frac{K1}{K2} \quad (3.35)$$

$$Kd_p = \frac{K3}{K2} \quad (3.36)$$

Fig.3-5 shows a block diagram of the entire control system for the vehicle body.

3.5 Fork Angle Disturbance Observer **(FDOB)**

In this section, we design an observer to estimate the disturbance applied to the fork angle. The equation of motion for the fork angle ÿf is given by (3.37) from (2.164) . However, g3 is the gravity term that affects the fork angle, and is given by (3.38) . Additionally, Tl f indicates the disturbance term including external force and friction.

$$m_{ÿ\,31ÿ¨w + m¯ÿ\,32ÿ¨p} + m¯_{ÿ\,33ÿ¨\,f + v¯_3'} + g3 = nf ÿf ÿ\, Tl\, f \tag{3.37}$$

$$g3 = mf\, lf\, g \cos ÿfÿp \tag{3.38}$$

Using the nominal value defined in equation (3.5) , equation (3.37) can be rewritten as equation (3.39) .

ÿ ˜ f on the right-hand side of $^{dis}_{(3.39)}$ is the total disturbance including the external disturbance term, internal interference force, gravity term, and inertial fluctuation. This is shown in equation (3.40) .

$$m_{ÿ\,n33ÿ¨_{f}^{res}} = nf\, ÿ\, f^{ref} - dis\, ÿ\, ÿ\, ˜\, f \tag{3.39}$$

$$ÿ^{dis} = m¯f\,{}'31\, ÿ¨^{res} + m¯_{ÿ\,32ÿ¨p^{res}} + (¯mÿ\, m\, 33\,{}'_{ÿ\, n33)ÿ¨f^{res}} + v¯_3' + g3 + Tl\, f \tag{3.40}$$

However, in order to suppress the amplification of high-frequency noise due to differentiation, a pseudo-detection method using a first-order low-pass filter is used. By differentiation, the estimated fork angle disturbance $ÿ^{dis}_{f}$ is calculated by equation (3.41) . Here, gf is used for FDOB. is the cutoff frequency of the low-pass filter.

$$ÿ^{dis}_{ˆ\, f} = \frac{gf}{f\, s + gf}\, ÿ^{dis}_{˜} \tag{3.41}$$

By rearranging equation (3.41) using equation (3.39) , the fork angle disturbance is given by equation (3.42) .

$$ÿ^{dis}_{ˆ\, f} = \frac{gf}{s + gf}\,\Big(nf\, ÿ_f^{ref} \quad n33ÿÿf\,)ÿs\,ÿf\,n33ÿÿ^{res} + gf\, m \Big) \tag{3.42}$$

Fig.3-6 shows the block diagram of the fork angle disturbance observer (FDOB) .

3.6 Reaction Torque Observer **(RTOB)**

In this section, we will discuss the repulsive compliance control (RCC) and the input of the compliance control. The reaction torque acting on the fork is estimated without using a force sensor or a torque sensor . In the RTOB used in this study , the reaction force $ÿ^{reac}_{f}$ Not only The reaction torque ÿ is calculated by adding the interference torque caused by the body and the wheels. $ÿ^{ext}_{f}$ Define it as:

Reaction torque $ÿ\, f^{ext}$ can be obtained as (3.43) by using (3.40) . $^{fric}_{f}$ indicates the friction torque that the fork receives, and is expressed as follows using the Coulomb friction Ff and the viscous friction coefficient Df :

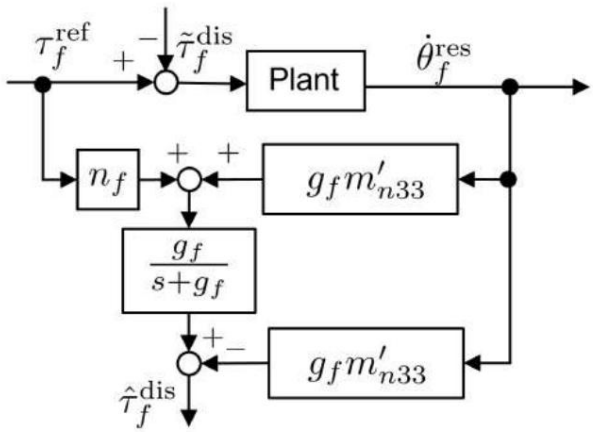

Fig. 3-6: Block diagram of the fork angle disturbance observer (FDOB)

In addition, since Tl f in equation (3.40) is a disturbance term including external forces and friction, it is divided as shown in equation (3.45) . It is assumed that.

$$\ddot{y}_f^{ext} = m^{-}_{'31}\ddot{y}^{res} + m^{-}_{\ddot{y}32\ddot{y}}{}^{res} + (^{-}m'_{\ddot{y}\,m\,33\,\ddot{y}\,n33)\ddot{y}}{}^{res}_{f} + v^{-}{}'_{+\,\ddot{y}\,3\,f}{}^{reac}$$

$$= nf\,\ddot{y}\,f^{ref}_{\ddot{y}\,m\quad\ddot{y}\,n33\ddot{y}}{}^{res}_{f}\;\ddot{y}\,g3\,\ddot{y}\,\ddot{y}\,f^{f\,ric} \tag{3.43}$$

$$f^{fric\,\ddot{y}} = Ff + Df\,\ddot{y}\ddot{y}_{f} \tag{3.44}$$

$$Tl\,f \quad f^{reac=\ddot{y}}_{f} + \ddot{y}\,f^{fric} \tag{3.45}$$

The fork angular acceleration ÿ¨ ff is calculated from the fork angular velocity ÿÿ by pseudo differentiation using a first-order low-pass filter. The reaction torque ÿˆ f is the cutoff frequency^{ext} can be calculated by formula (3.46) , where gr f is used for RTOB . of the low-pass filter.

$$\ddot{y}\hat{}f^{ext} = \frac{gr\,f}{s + gr\,f}\left(\mathbf{nf}\,\ddot{y}\,f^{ref}_{res} + gr\,f\,m\ddot{y}\,n33\ddot{y}\ddot{y}\quad\ddot{y}\,g3\,\ddot{y}\,\ddot{y}\,f^{f\,ric}\right)\ddot{y}\,gr\,f\,m\,\ddot{y}\,n33\ddot{y}\ddot{y}\,f^{res} \tag{3.46}$$

Fig.3-7 shows the block diagram of the reaction force estimation observer (RTOB) .

3.7 Compliance Control

In this section, we will discuss compliance control applied to the fork.

Compliance control is applied to mitigate the shock to the transported object by moving the forks in accordance with the external force applied to the fork or the inertial force from the body or wheels.

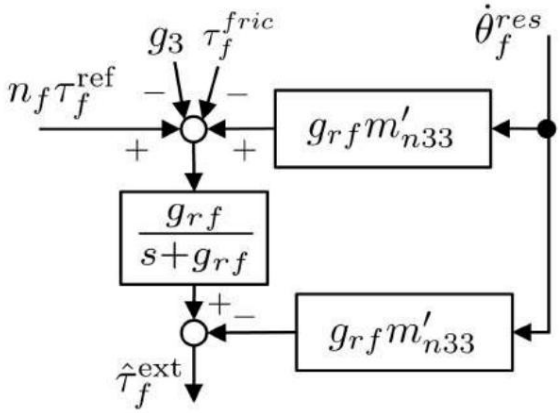

Fig. 3-7: Block diagram of reaction force estimation observer (RTOB)

The input is the estimated reaction torque ÿˆ obtained from the RTOB of the fork, as described in Section 3.6. $\hat{\tau}_f^{ext}$ We use

However, because the external force acting on the forks includes the gravity due to the mass of the transported object, if the value of ÿˆ ext is

used as is, there is a high possibility that the forks will always tilt in accordance with the weight of the transported object, causing the object to drop.

Therefore, it is dangerous to use it for transportation.

It is necessary to subtract the DC component, such as the gravity due to the mass of the transported object, from the external force applied to the load.

In this study, the input ÿˆ f $\dot{\hat{\tau}}_f^{ext}$ Use a first-order high-pass filter.

It is calculated by equation (3.47) , where gh is the cutoff frequency of the high-pass filter.

$$\dot{\hat{\tau}}_f^{ext} = \frac{s}{s + g_h}\,\hat{\tau}_f^{ext} \tag{3.47}$$

The input ÿˆ f calculated by equation $\dot{\hat{\tau}}_f^{ext}$ (3.47) Virtual impedance model for compliance control using

The delta is shown in equation (3.48) .

$$M_{cc}\ddot{y}_{fc}^{cmd} + D_{cc}\dot{y}_{fc}^{cmd} + K_{cc}y_{fc}^{cmd} = A_{cc}\dot{\hat{\tau}}_f^{ext} \tag{3.48}$$

Mcc, Dcc, and Kcc represent the virtual inertia, viscosity, and stiffness coefficients, respectively. Acc represents the assist gain of the external force.

By using equation (3.48) , the command values of the fork angle, angular velocity, and angular acceleration, y_{fc}^{cmd}, $\dot{y}_{fc}^{cmd}$,

$\ddot{y}_{fc}^{cmd}$ is generated. The command value is y_{fc}^{cmd} and $\dot{y}_{fc}^{cmd}$ are used to make the fork follow the command value .

This enables the robot to move in accordance with disturbances and absorb the shocks that the transported object receives . Fig. 3-8 shows a block diagram of compliance control.

The transfer function between the input torque and the pitch angle command value is a second-order delay system, similar to the transfer function of the RCC.

The characteristics are the natural angular frequency ÿf , the damping ratio ÿf , and the gain Gcc , which is a coefficient that determines the magnitude of the output.

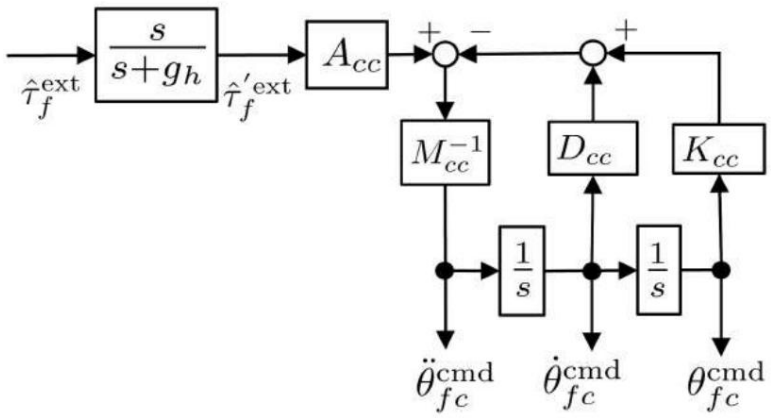

Fig. 3-8: Compliance Control (CC) Block Diagram

Using this, it is shown by equation (3.49) . Each coefficient can be calculated from equation (3.50) to equation (3.52) .

$$\frac{}{\text{cmdÿfcÿext ÿ˜f}} = \frac{\text{Gccÿf}^{2}}{^{2s} + 2\ddot{y}\,f\ddot{y}f\,s + \ddot{y}\;\overline{\;\;\;}^{2}_{f}} \tag{3.49}$$

$$\ddot{y}f = \ddot{y}\mathbf{Kcc}\,\overline{\text{Mcc}} \tag{3.50}$$

$$\ddot{y}\,f = \frac{}{\text{DCC }\overline{2\ddot{y}\text{MCC}}} \tag{3.51}$$

$$\text{Gcc} = \frac{\text{Kcc}}{\text{Acc}} \tag{3.52}$$

The method for determining each parameter is the same as for RCC, in order to prevent resonance and speed up the response.

The damping ratio ÿ f is set to 1. It is desirable to set the natural angular frequency ÿ f large in order to make the reaction faster and to deal with disturbances in a wide range. In addition, when compliance control is activated, the fork tilts from a horizontal position with respect to the ground, so the gain Gcc , which is the coefficient that determines the magnitude of the output , is set to 1.

It is desirable to set the impact of the shock on the transported goods within an acceptable range.

3.8 Fork angle command generator

In this section, we describe the fork angle command generator for a two-wheeled mobile transport robot.

In order for the transported goods to remain stable and not fall, the forks must be horizontal to the ground.

The angle of the fork with respect to the ground is ÿfÿp , which is the fork angle minus the pitch angle . Therefore, in the absence of disturbance, the command value of the fork angle is equal to the response value of the pitch angle.

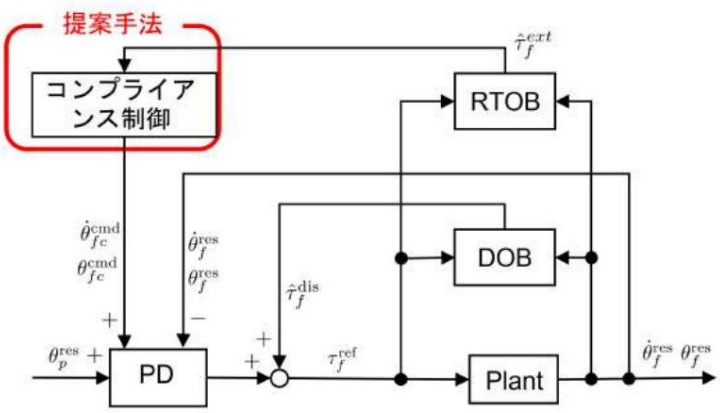

Fig. 3-9: Block diagram of the entire control system for the fork

The fork angle command value obtained by compliance control is added.

Angle command value $\ddot{y}_f^{cmd}$ is found as equation (3.53) .

$$\ddot{y}_f^{cmd} = \ddot{y}_{fp}^{cmd} + \ddot{y}_{fc}^{res} \tag{3.53}$$

In order for the transported object to be stable, it is desirable for the fork angular velocity to be 0 .

In this study, the fork angular velocity command value $\ddot{y}_f^{cmd}$ was calculated by compliance control.

This coincides with the time value, and equation (3.54) holds.

$$\ddot{y}_{ffc}^{cmd} = \ddot{y}_f^{cmd} \tag{3.54}$$

PD control is performed using the fork angle command value calculated by equations (3.53) and (3.54) , and the fork angle command value is calculated by the following formula in Section 3.5 .

The fork angle disturbance $\hat{y}_f^{dis}$ By compensating for this, the fork torque reference value $\ddot{y}_f^{ref}$ is calculated using equation (3.55) .

$$\ddot{y}_f^{ref} = Kp_f(\ddot{y}_f^{cmd} - \ddot{y}_f^{res}) + Kd_f(\dot{\ddot{y}}_f^{cmd} - \dot{\ddot{y}}_f^{res}) + \frac{\hat{y}_f^{dis}}{n_f} \tag{3.55}$$

Here, Kp_f and Kd_f respectively indicate the proportional gain and the differential gain. Fig.3-9 shows a block diagram of the entire control system in the fork.

Chapter **4**

experiment

In this section, we will describe the experiment. In section 3 , we explained a method to reduce the shock generated by the wheels when the robot moves forward and backward and transmitted to the transported object .

In Section 4.1, we verified that the real-world control can reduce the impact.

In Section 4.2, we explain the outline of the experiment. In Section 4.3, we present the experimental results.

The results are explained below.

4.1 Setting the coordinate system for the transported item

First, define the coordinate system of the transported object. Define the luggage coordinate system ÿL{XL, YL, ZL} at the center of gravity of the transported object.

From the perspective of the fork coordinate system ÿf, ÿL is located at a point translated lL in the Xf direction and lG in the Zf direction. The diagram of the transported object on a two-wheeled mobile transport robot is shown in Fig. 4-1 .

4.2 Experimental overview

In this section, we will outline the experiment. The two-wheeled mobile transport robot used in the experiment is shown in Fig. 4-2.

In this paper, we conducted experiments assuming that the wheels were equipped with chains.

The unevenness was created by attaching plastic pieces about 1 mm thick at 5 cm intervals to the outer circumference of the

The wheel is shown in Fig. 4-3 .

The physical parameters used in this experiment are shown in Table 4.1, and the control parameters are shown in Table 4.2 .

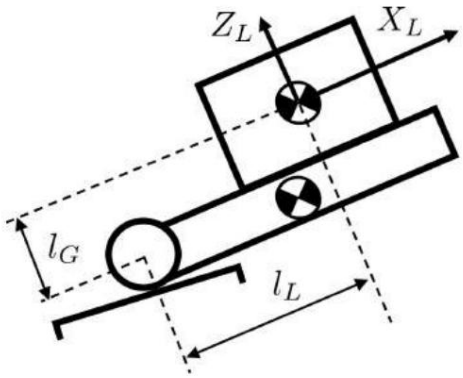

Fig. 4-1: Parts of the transported object in a two-wheeled mobile transport robot

Fig. 4-2: The two-wheeled mobile transport robot used

The flow of the experiment is explained below. First, the two-wheeled mobile transport robot was turned upside down, and then the transported object shown in Fig. 4-4 was placed on it. Sensors were included in the transported object to measure the translational acceleration and angular acceleration of the transported object. Since the transported object was placed on the forks by a person, it was difficult to adjust the impact when it was placed on the forks evenly.

Therefore, in order to reduce the effect of carrying a load on the forks and the vehicle body posture,

For the purpose, the vehicle was stopped in place for 12 seconds. After that, the speed was reduced to 0.25 m/sec and the maximum acceleration was reduced to 0.25 m/sec2.

The robot was then set to the same speed and maximum acceleration as when it was moving forward, and moved forward 1.5 m. After stopping the robot for 6 seconds, the robot was moved forward at the same speed and maximum acceleration as when it was moving forward.

The vehicle was then moved backwards 1.3 m .

The conventional method uses only the response value of the pitch angle as the fork angle command value, and the proposed method uses the

Fig. 4-3: Wheels used in the experiment

A comparison was made with a case where compliance control was used for the fork.

Table 4.1: Physical parameters used in the experiment

item	Unit Value	
Weight of body mb	kg	43.1
Weight of wheels	kg	1.21
mw Weight of forks mf	kg	2.0
Mass of transported	kg	3.74
object mL Moment of inertia of body around y -axis	kg/m2	1.02
Iyy Moment of inertia of wheels around y -axis Iwy	kg/m2	3.40 × 10ÿ3
Moment of inertia of the wheel rotor around the y- axis Iry	kg/m2	4.50 × 10ÿ5
Moment of inertia of the fork about its y -axis If y	kg/m2	0.347
Moment of inertia of the fork rotor about its y -axis If ry	kg/m2	2.61 × 10ÿ5
Wheel radius R	m	0.075
Body height L	m	0.276
Body center of gravity	m	0.22
height l Fork center of	m	0.275
gravity height lf		11
Wheel gear ratio nw Fork gear ratio nf		31

Table 4.2: Control parameters used in the experiment

Item	Unit	Value
Proportional gain Kpw in tracking control Integral	-	4.5
gain Kiw in tracking control Proportional gain	-	0.6
Kpp in attitude stabilization control Differential gain Kd in	-	200
attitude stabilization control p	-	20ÿ2
SPADO cutoff frequency gs	Hz	4
Virtual inertia Mrcc of RCC	-	0.137
Virtual Viscous Drcc of RCC	-	1.549
Virtual stiffness Krcc of RCC	-	4.381
FDOB cutoff frequency gf	Hz	5
RTOB cutoff frequency gf	Hz	15

Fig. 4-4: Transported items used in the experiment

4.3 Experimental results

This section shows the results of the experiments.

First, the acceleration in the XL direction of the transported object in the conventional method and the proposed method are shown in Fig. 4-5, The time is shown in Fig. 4-6 . In the following figures, the time when the robot starts moving forward is set as 0 seconds.

As shown in Fig. 4-5 and Fig. 4-6 , the peak acceleration can be reduced both when moving forward and backward. It can be seen that the peak acceleration can be suppressed especially when reversing.

The forks move in response to disturbances, reducing the impact on the transported goods.

In addition, the proposed method showed a larger acceleration than the previous method except when moving forward or backward.

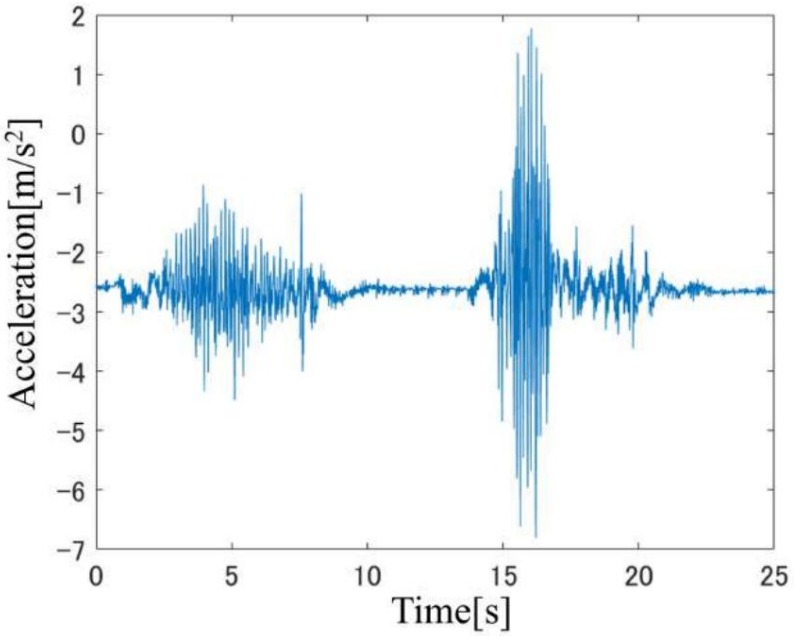

Fig. 4-5: Acceleration of the transported object in the XL direction in the conventional method

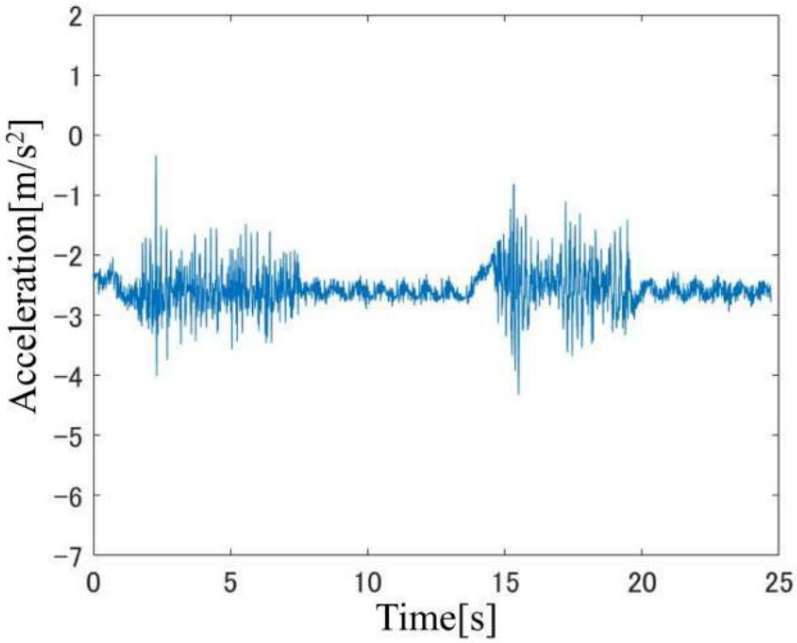

Fig. 4-6: Acceleration of the transported object in the XL direction in the proposed method

It can be seen that the off-axis speed is ÿ2.6 m/s . This is thought to be due to the fact that the influence of the disturbances received during forward and reverse driving continues .

This is thought to be due to the effect of gravity caused by the inclination of the forks relative to the ground .

These are shown in Fig. 4-7 and Fig. 4-8 , respectively .

In both Fig. 4-7 and Fig. 4-8 , the maximum value is observed in the range of 5 to 10 Hz .

It can be confirmed.

The reason why the maximum frequency is around 5 to 10 Hz is explained.

The robot was moved at a speed of 0.25 m/sec both when moving forward and backward . Therefore, disturbances due to unevenness were generated five times per second from only one wheel.

In addition, if the timing at which the two wheels cross the plastic piece is different, the wheel

The disturbance caused by unevenness occurs 10 times per second . Therefore , the spectrum has a maximum between 5 and 10 Hz .

It is assumed to take on a value.

In addition, Fig. 4-7 and Fig. 4-8 show that the effects of acceleration have been improved at all frequencies.

Both the conventional method and the proposed method have large values near 0 Hz , but this is due to gravity.

This is thought to be due to the existence of an offset caused by the

Next, the acceleration of the transported object in the ZL axis direction in the conventional and proposed methods is shown in Fig. 4-9 and Fig. Shown in 4-10 .

From Fig. 4-9 and Fig. 4-10 , in both forward and reverse motion, the ZL axis direction is the same as the XL axis direction.

It can be seen that the peak acceleration in the forward direction is reduced.

It can be seen that the speed is being reduced.

offset of about 2 in the XL axis direction, the velocity of the conventional method and the proposed method was 9.6 m/s. As in the case of an

It has a.

Power spectrum solution of the ZL axis acceleration of the transported object in the conventional and proposed methods

The analyses are shown in Fig. 4-11 and Fig. 4-12 , respectively.

In Fig. 4-11 , it can be seen that the maximum value is around 9 Hz , which is due to the unevenness of the wheel.

From Fig. 4-11 and Fig. 4-12 , it is considered that the same phenomenon occurs at all frequencies as in the case of the XL axis direction .

It can be seen that the effect of acceleration is reduced in both cases. Both have large values near 0 Hz due to the offset caused by gravity.

Next, the angular acceleration of the transported object around the YL axis in the conventional method and the proposed method are shown in Fig. 4-13 and Fig . 4-14 , respectively. As in the case of the acceleration in the XL axis direction and the acceleration in the ZL axis direction ,

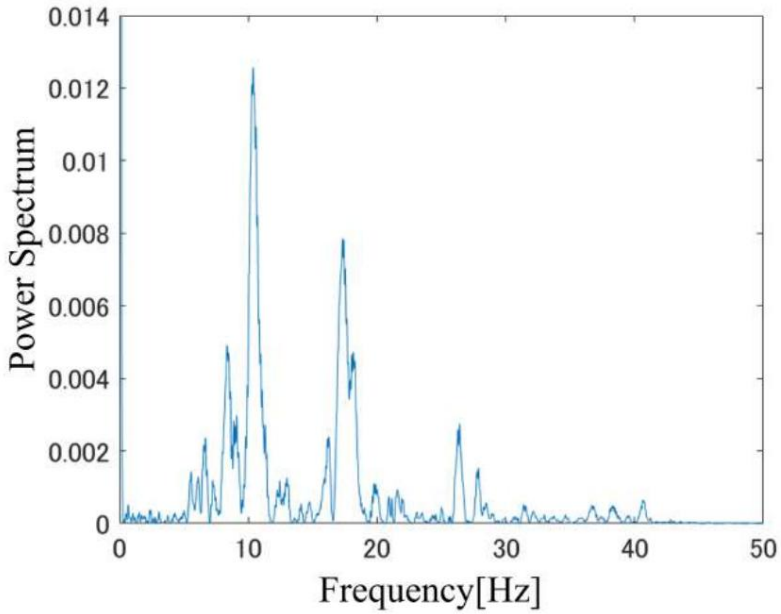

Fig. 4-7: Power spectrum analysis of the acceleration in the XL direction of the transported object in the conventional method

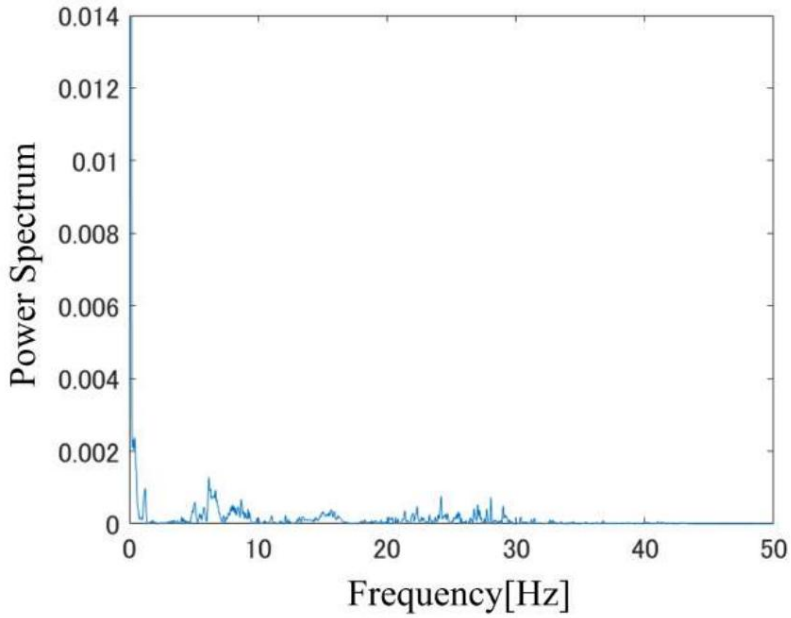

Fig. 4-8: Power spectrum analysis of the acceleration in the XL direction of the transported object in the proposed method

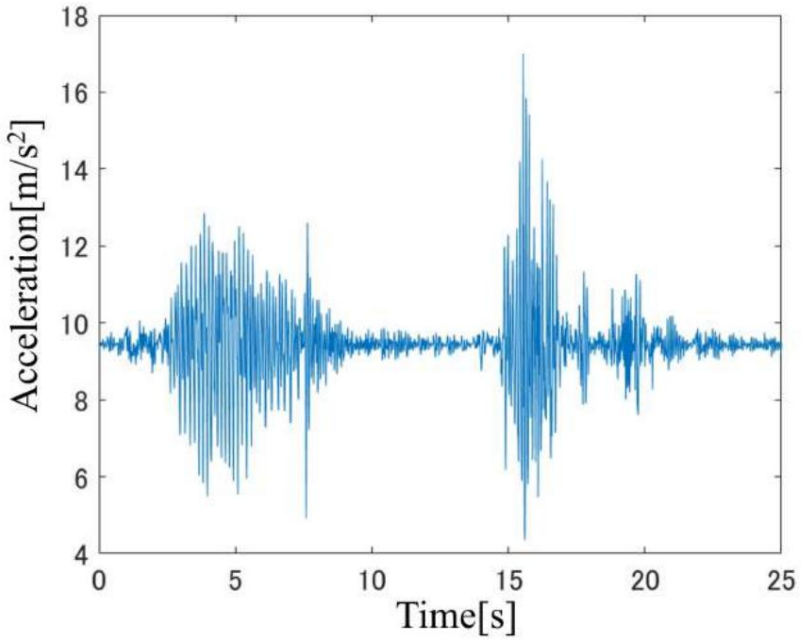

Fig. 4-9: Acceleration of the transported object in the ZL axis direction in the conventional method

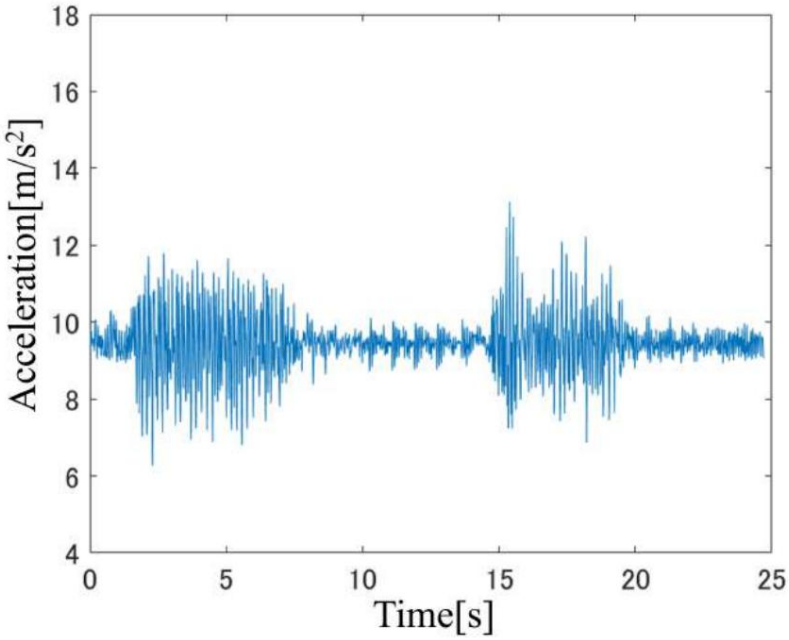

Fig. 4-10: Acceleration of the transported object in the ZL axis direction in the proposed method

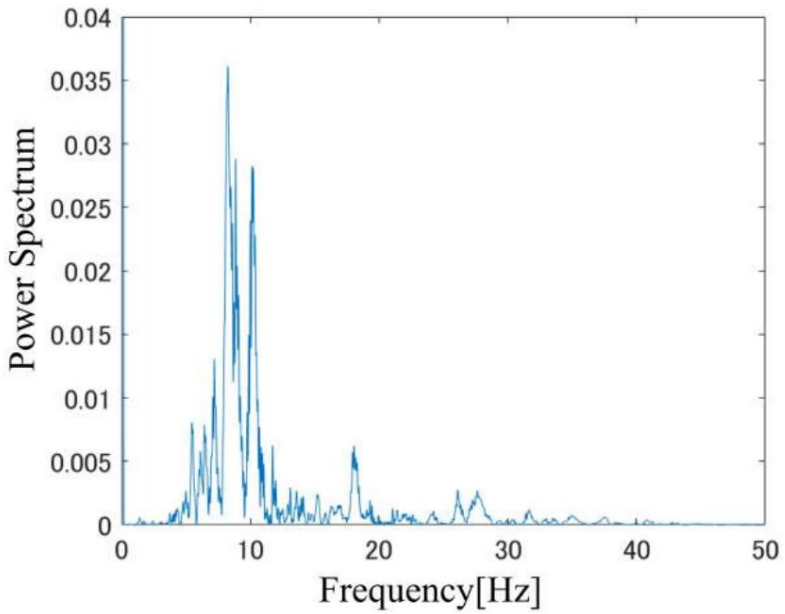

Fig. 4-11: Power spectrum analysis of the acceleration in the ZL axis direction of the transported object in the conventional method

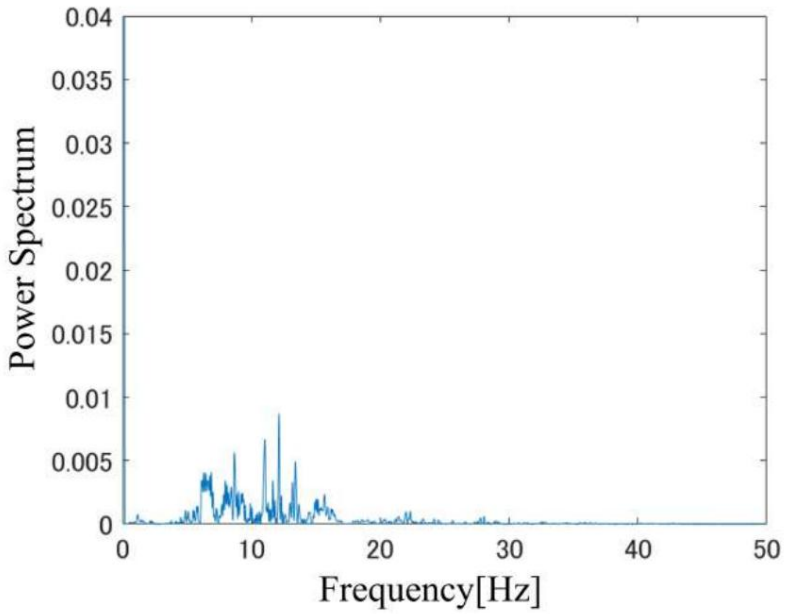

Fig. 4-12: Power spectrum analysis of the acceleration in the ZL axis direction of the transported object in the proposed method

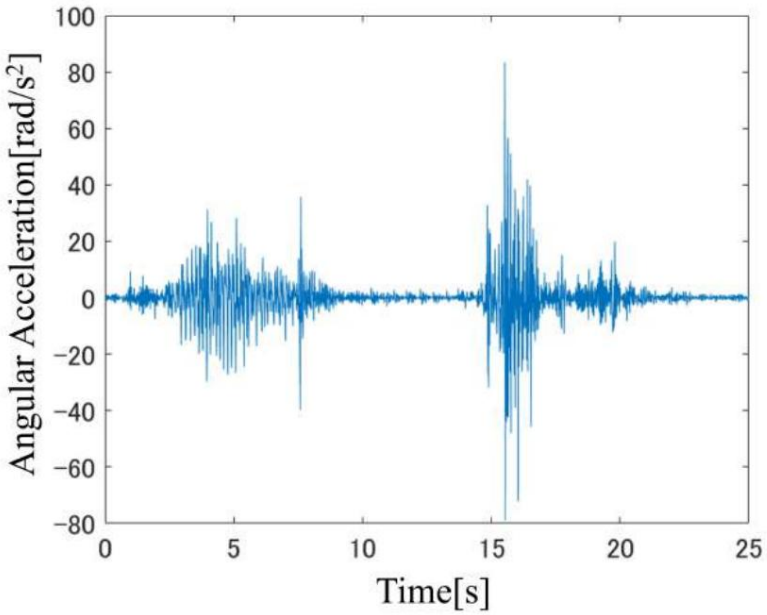

Fig. 4-13: Angular acceleration of the transported object around the YL axis in the conventional method

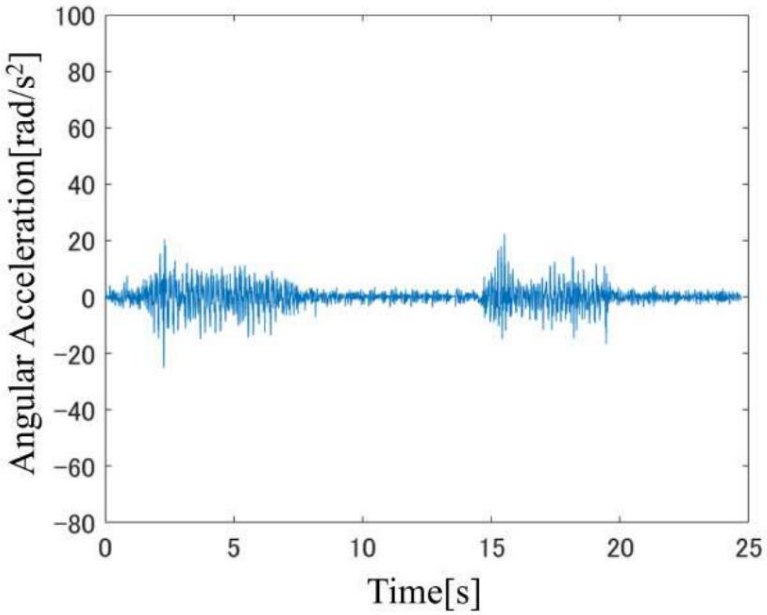

Fig. 4-14: Angular acceleration of the transported object around the YL axis in the proposed method

In addition, the peak angular acceleration around the YL axis is also reduced both when moving forward and backward.
It can be confirmed that the peak acceleration can be suppressed especially when reversing.
It can be confirmed that

Power spectrum of the angular acceleration around the YL axis applied to the transported object in the conventional and proposed methods
The analysis results are shown in Fig. 4-15 and Fig. 4-16 , respectively .

From Fig. 4-15 , the 5 to 10 Hz range is considered to be due to disturbances caused by unevenness in the wheels.
In addition to the value in minutes, it is clear that the values are large in the 15 to 20 Hz and 25 to 30 Hz ranges.
This is thought to be due to the effect of fork resonance.

Since the actual machine is a two- degree-of-freedom system consisting of a body and fork, it has two natural frequencies. Therefore, the 15 to 20 Hz and 25 to 30 Hz ranges are considered to correspond to the resonant frequencies. Fig. 4-15 and Fig. 4-16 show that not only the effects of disturbances caused by the wheels but also the effects of resonance have been reduced.
It can be confirmed that

Next, the pitch angle ÿp, fork angle ÿf, and their difference ÿfÿp in the conventional and proposed methods are shown in Fig. 4-17 and Fig. 4-18 , respectively . Here, the difference between the pitch angle and the fork angle ÿfÿp is the fork angle relative to the ground.
This indicates the slope of the curve.

From Fig. 4-17 and Fig. 4-18 , it can be confirmed that the inverted state can be maintained even when the proposed method is used.
Compared to the conventional method, the inclination of the fork with respect to the ground increases in the proposed method, but the transport
No problems that would impede transportation, such as items falling, were observed.

Therefore, the proposed method does not affect transportation in terms of posture stabilization control.
was shown.

Finally, the orbital responses for the conventional method and the proposed method are shown in Fig. 4-19 and Fig. 4-20 , respectively.

From Fig. 4-19 and Fig. 4-20 , it can be seen that the tracking performance is improved when the proposed method is used compared to the conventional method. At 0 seconds, there is a discrepancy between the command value and the experimental value, but when the transported object is loaded,
This was caused by a misalignment that occurred when the vehicle moved forward and did not return to its original position even after a period of time had passed.
Therefore, it is possible to drive the vehicle according to the command value even when the proposed method is used.
was shown.

From the results of Fig. 4-5 to Fig. 4-20 , the proposed method reduces the impact on the transported object compared to the conventional method.
It has been shown to be effective in reducing

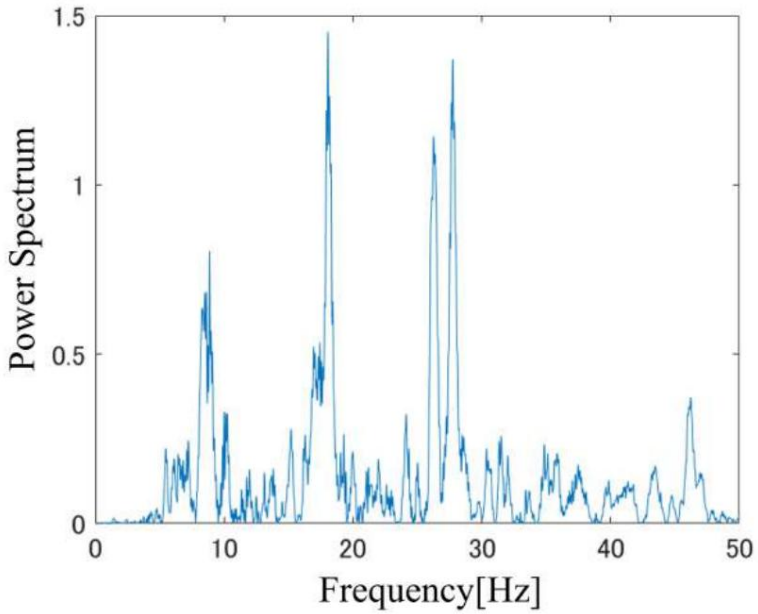

Fig. 4-15: Power spectrum analysis of the angular acceleration of the transported object around the YL axis in the conventional method

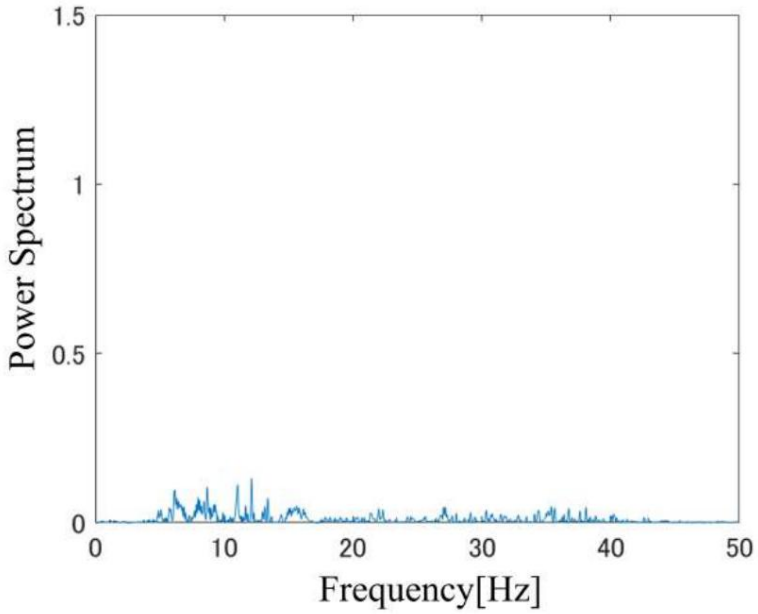

Fig. 4-16: Power spectrum analysis of the angular acceleration of the transported object around the YL axis in the proposed method

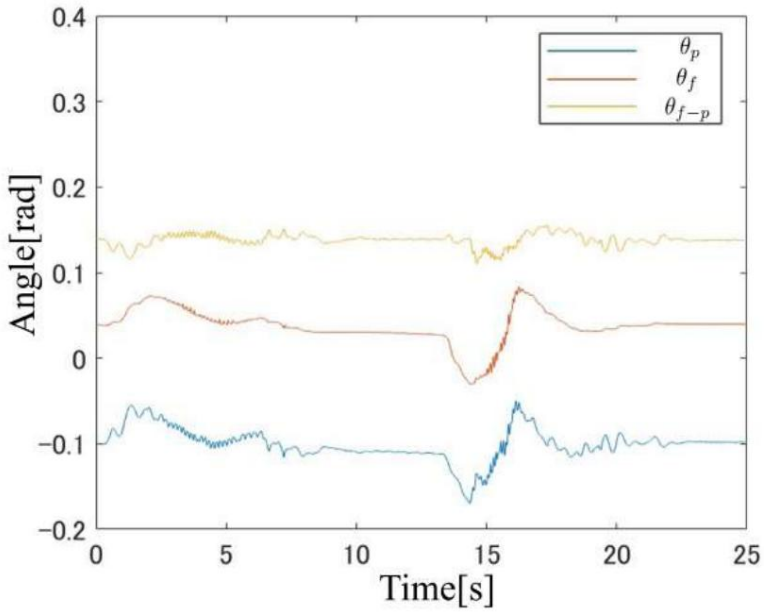

Fig. 4-17: Pitch angle and fork angle response in the conventional method

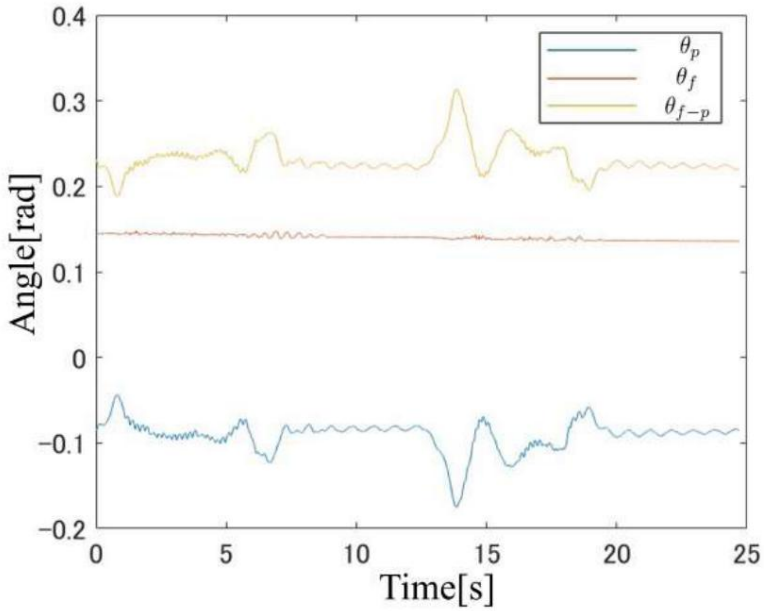

Fig. 4-18: Pitch angle and fork angle response in the proposed method

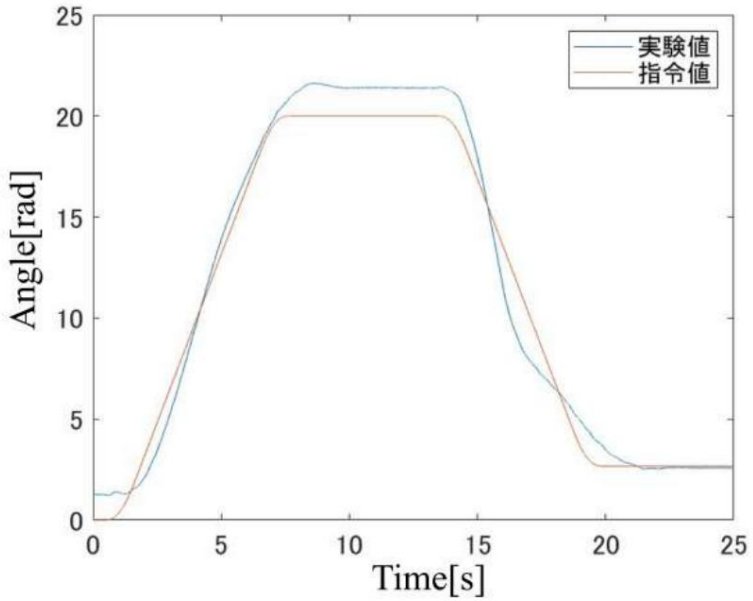

Fig. 4-19: Orbit response in conventional method

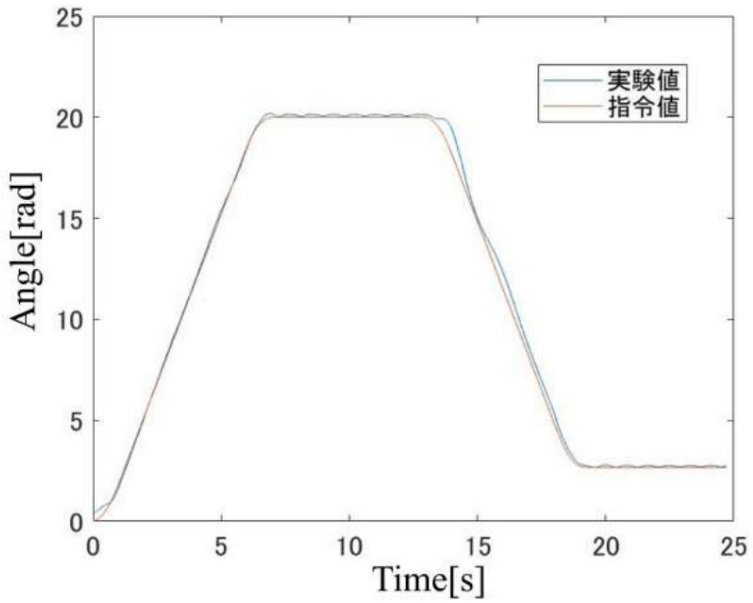

Fig. 4-20: Orbit response in the proposed method

Chapter **5**

Conclusion

In this study, we aimed to suppress the impact on the transported object of a two-wheeled mobile transport robot by using a compliance We proposed a virtual suspension control using inequality control.

Compliance control is used to control the fork to move in accordance with the force, and the transport The impact of the conveyed goods was suppressed. In addition, the input of the compliance control was adjusted to prevent the fork from continuing to tilt. To prevent this, a high-pass filter was used to remove the DC component from the value output by the RTOB . I used something.

In this study, the effectiveness of the proposed method was verified through experiments. In the experiments, it was confirmed that the peak values of the translational acceleration and angular acceleration of the transported object were reduced by the proposed method. It was shown that the impact of shock on the transported goods was suppressed by this. From the results of the trajectory response and the trajectory response, the posture stabilization of the two-wheeled mobile transport robot was It was shown that this has no effect on control and tracking control.

Future challenges are listed below.

- Parameter design according to the weight of the transported goods
- Check and improve performance when turning

The first issue is parameter design when the weight of the transported object differs. There are many parameters that can be set arbitrarily in the transport and compliance control.

Since the value output to the RTOB changes depending on the weight of the object , it is thought that the behavior of the control system will change.

It is considered necessary to develop a method for determining parameters that correspond to the weight of the transported object, and this is set as a future task.

The second issue is to confirm and improve the performance of the robot when it turns. In this paper, we assumed that the robot moves only in a straight line. However, in actual logistics sites,

When using a robot, turning motion is necessary. Therefore, the effectiveness of the proposed method in turning motion is

It is necessary to analyze the above and improve the parameter settings and mechanism, which is a future task.

Appendix **A**

Specifications of the experimental aircraft

This chapter describes the specifications of the experimental machine.

A.1 Motor and motor driver specifications

The specifications of the wheel and fork motors used in the experimental machine are shown in Tables A.1 and A.2 . The specifications of each motor driver are shown in Table A.3 and Table A.4 .

Table A.1: Specifications of the motor used in the wheels

Type	AC Servo Actuator
Manufacturer Model	Harmonic Drive Systems Inc.
	HPG-20A-11-J6GDK
Instantaneous maximum	217 Nm
torque Rated	20 Nm
torque Average load	45 Nm
torque Peak torque when stopped on	100 Nm
track Reduction ratio	11

Table A.2: Specifications of the motor used in the fork

Type	AC Servo Actuator
Manufacturer Model	Harmonic Drive Systems Inc.
	HPG-32A-33-J2NELA
Instantaneous maximum	650 Nm
torque Rated	108 Nm
torque Average load	200 Nm
torque Peak torque when stopped on	300 Nm
track Reduction ratio	33

Table A.3: Specifications of the motor driver used for the wheels

kinds	AC Servo Driver
Manufacturer: Omron Corporation	
Model R88D-1SN04L-ECT	
Rated output current	4.8 A
Maximum output	14.7 A
current Input power voltage	Single-phase AC100 to AC120 V
Command	DC24V
input Mass	1.9 kg

Table A.4: Specifications of the motor driver used in the fork

Type AC servo driver	
Manufacturer: Omron Corporation	
Model R88D-KN04L-ECT	
Rated output current	4.6 A
Maximum output current	19.5 A
Input power voltage:	Single-phase AC100 to AC120 V
Command input:	Single-phase AC100 to AC120 V
Mass 1.6 kg	

A.2 Sensor Specifications

The specifications of the encoder used to obtain the vehicle pitch angle information are shown in Table A.5 . The specifications of the smartphone used as the acceleration sensor are shown in Table A.6 .

Table A.5: Specifications of the encoder used to obtain vehicle pitch angle information

Manufacturer	Baumer Corporation
Model	EIL580P-SC
Encoder type Incremental encoder	
Resolution 65536 pulses/revolution	

Table A.6: Smartphone specifications

Manufacturer: Apple	
Model name: iPhone SE	
iOS version 16.1.2	
Output Period	100Hz

References

[1] Ministry of Economy, Trade and Industry, Commerce and Information Policy Bureau, Information Economy Division,

"Market research report on electronic commerce in fiscal year 2021,"

https://www.meti.go.jp/press/2022/08/20220812005/20220812005-h.pdf (Reference 2023

(January 21st) .

[2] CBRE,

"Tenant Survey on Logistics Facility Usage 2022,"

https://cbre.vo.llnwd.net/grgservices/secure/Japan_Logistics%

20Occupier%20Survey_June%202022_JP_D162.pdf?e=1674275029&h=

da87ce156e6bfdd4627d37b525ac99bb (Referenced January 21 , 2023) .

[3] Yano Research Institute,

"Research conducted on the AGV/AMR (transport robot) market (2022),"

https://www.yano.co.jp/press-release/show/press_id/3047#:˜:text=AGV%2FAMR%

EF%BC%88,%E5%B9%B4%E5%BA%A6%E3%82%92%E4%B8%8B%E5%9B%9E%E3%81%A3%E3%81%9F%

E3%80%82 (Referenced January 21 , 2023) .

[4] Toyota L&F,

"Unmanned Forklift - Product Information,"

http://www.toyota-lf.com/products/detail/pilotless_forklift/index.html (Referenced January 21 , 2023) .

[5] MUJIN Inc. ,

"MUJIN AGV (Automated Guided Vehicle),"

https://www.mujin.co.jp/solution/mobilerobot/agv/ (Referenced January 21 , 2023).

[6] Kenji Mikoda,

"Prevention of Condensation Based on Case Studies,"

Obayashi Technology Research Institute Bulletin Edited by Obayashi Technology Research Institute (72), 1-8, 2008.

[7] Concrete Medical Center,

"How to protect exposed concrete walls from the cold,"

https://concrete-mc.jp/uchippanashi-wall/#4 (Referenced January 21 , 2023) .

[8] J-Works,

"Adak I -type ring tire chain for construction special vehicles ,"

http://hodumi.co.jp/jworks/sp/item/?id=2068 (Referenced December 25 , 2022).

[9] Segway-Ninebot,

“Segway X2 SE , ”

https://ap-en.segway.com/product/segway-x2-se.html (Referenced January 21 , 2023).

[10] Toyota Motor Corporation,

"Winglet (Type L),"

https://global.toyota/jp/download/11466448/ (Referenced January 21 , 2023) .

[11] Ministry of Economy, Trade and Industry, Ministry of Land, Infrastructure, Transport and Tourism, Ministry of Agriculture, Forestry and Fisheries,

"The current situation surrounding logistics in Japan and the status of initiatives,"

https://www.meti.go.jp/shingikai/mono_info_service/sustainable_logistics/

pdf/001_02_00.pdf (Referenced January 19 , 2023).

[12] F. Grasser, A. D' Arrigo, S. Colombi, and A.C. Rufer,

``Joe: a mobile, inverted pendulum,''

IEEE Transactions on Industrial Electronics, Vol. 49, No. 1, pp. 107-114, 2002.

[13] K. Pathak, J. Franch, and SK Agrawal,

“Velocity and position control of a wheeled inverted pendulum by partial feedback linearization,”

IEEE Transactions on Robotics, Vol. 21, No. 3, pp. 505-513, 2005.

[14] A. Nakamura and T. Murakami,

"
A stabilization control of two wheels driven wheelchair,”

2009 IEEE/RSJ International Conference on Intelligent Robots and Systems, pp. 4863-4868, 2009.

[15] Kohei Onishi,

"Robust Motion Control Using Disturbance Observer,"

Journal of the Robotics Society of Japan, Vol. 11, No. 4, pp. 486-493, 1993.

[16] T. Kuramatsu and T. Murakami,

“Force sensorless power-assist control of yaw motion direction for two wheels driven wheelchair,”

In 2010 World Automation Congress, pp. 1-6, 2010.

[17] Kim Byung-Gyu,

" Robust Posture Stabilization Control of a Two- Wheel Drive Electric Wheelchair,"

Master's thesis, Graduate School of Science and Technology, Keio University, 2011.

[18] Naoya Hatakeyama, Akira Shimada,

" High-speed movement control of an inverted pendulum using Zero

Dynamics," Transactions of the Society of Instrument and Control Engineers,

Vol.42, No.9, pp. 1035-1041, 2006.

[19] Naoya Hatakeyama, Akira Shimada,

"High-speed movement control of an inverted pendulum type mobile robot considering robustness,"

Transactions of the Society of Instrument and Control Engineers,

Vol.44, No.9, pp. 721-728, 2008.

[20] OK Sayidmarie, MO Tokhi, and SA Agouri,

"
Impact of dynamically moving payload on two wheeled robot stability,”

19th International Conference on Methods and Models in Automation and Robotics (MMAR), pp.

915-920, 2014.

[21] Daisuke Sekiguchi,

" Robust Driving Control of Two-Wheeled Mobile Robot Considering Weight and Center of Gravity Changes Due to Cargo,"

Master's thesis, Graduate School of Science and Technology, Keio University, 2021.

Acknowledgements

We would like to express our sincere gratitude to Professor Toshiyuki Murakami for his kind guidance throughout this research.
Thank you for taking the time to join the discussion despite your busy schedule.
I will do my best to respond appropriately to any questions or concerns, including irrelevant questions due to my lack of knowledge.
Thanks to their support, I was able to continue my research without giving up.
I received various opinions from my professors during the midterm presentations and the SUM training camp. They pointed out areas where my thoughts were lacking or that I had not considered in each presentation, which helped me to improve my research.
I am very grateful.

I would like to express my sincere gratitude to my senior colleagues in the lab who have been so kind to me throughout my time in the lab.
My senior doctoral students have a lot of knowledge and have given me a lot of advice, not just about control.
I would like to thank Keita Shimamoto for helping me understand the points that I was not able to understand during the whole group and group discussions.
I received advice on my research during the interim presentation and related knowledge.
I received a lot of advice on my presentation and warm support for my research.

I am grateful to my seniors in the second year of the master's program for their help. I was also grateful to Mitsuru Yajima, who has a similar research theme.
I was very grateful for the help I received from the team, as they were using the same actual machine.
He kindly answered my questions about control.
When I was in the lab, he was always available to help me .
I think that they came to our store and told us many different stories, which gave me the opportunity to become friends with the seniors.
Hiroki Morishita gave me a lot of advice during seminars and other events. Daisuke Yanagibe gave me a lot of advice about studying abroad. He also accompanied me on walks.
I consulted with him on various matters, including research-related matters.
When I was having trouble with my research, he was willing to give me advice, even though we are in different fields.

I was also very grateful to my first- year master's students. Hirotake Kanazawa taught me how to use the machine.
Despite his busy schedule, he answered questions about his research.

He taught me how to write a resume and gave me a lot of encouraging words while I was writing my thesis.

I had a great time talking to Tomoaki Baba in the lab. I also had a great time talking to Kazuto Muto in the group.

During the lecture, he gave me feedback on my slides. During the second semester, he also came from Italy to check on my research progress and life.

Through the peer review, I received advice on research and how to write a paper.

We would like to thank Yusuke, Kazuki Iene, Yuri Sawane, and Erika Takeuchi for their help in discussing the research.

He also gave me a lot of advice during seminars and SUM training camps.

Luc Vignolles , Theo-Gabriel Gilles , Litong Huang , Elea Papin , and Pavia Matteo

I would like to thank Ms. Dethoor Lucas and Ms. Maria Sanchez Garbayo . I am not good at English and had to ask them to repeat themselves many times, but I was able to have many conversations and learn about a world I had never known before.

I would also like to thank my lab classmates, Hitoshi Ito and Kubota, who I spent the past year with.

Mr. Koichirou, Mr. Naoki Tsuda, Ms. Hatsudai Ayori, Mr. Hiroaki Katagiri, Mr. Tadakiyo Kotani, and Mr. Take

I would like to thank Itake-kun, Yuhei Tomioka-kun, and Shigeki Yashita-kun. Over the past year, I have worked with them on the SUM training camp, the midterm presentations,

I was able to overcome the difficult times, such as writing my graduation thesis, thanks to my classmates.

We went out to eat together and had many conversations in the lab, and it was a very fulfilling lab life.

Thank you very much. Finally, I would like to thank my family for always supporting me and watching over me with kindness.

I would like to express my sincere gratitude to the family. Thank you very much.

January 25 , 2023